RSC Advances

REVIEW

Cite this: *RSC Adv.*, 2020, **10**, 16431

Fundamentals and recent progress relating to the fabrication, functionalization and characterization of mesostructured materials using diverse synthetic methodologies

Soroush Soltani, *[a] Nasrin Khanian,[b] Umer Rashid[c] and Thomas Shean Yaw Choong[a]

Since 1990 and the invention of the very first generation of ordered mesoporous silica materials, several innovative methodologies have been applied to synthesize, characterize, and modify silica/non-silica mesoporous materials. The growth of the mesoporous materials field has generated significant environmental and economic advantages compared to various other industrial developments. According to the literature, there are several key synthesis approaches and parameters that can affect the structural, textural and morphological characteristics of mesoporous materials. To date, huge attempts have been made to maximize the activities and selectivities of these materials through either the *in situ* or post-synthesis functionalization of the large interior surface areas and internal mesostructured frameworks in the presence of specific organic/inorganic components. However, the main challenge is to provide good control over the incorporation and distribution of multiple guest components within the mesostructured hosts. Mesostructured materials have received great attention for various applications, such as being used in electronics, medicine, photocatalysis, catalyst supports, catalysis, absorbers, sensors, gas separation, *etc.* In the current paper, several recent developments have been highlighted and reviewed regarding the fabrication and characterization of siliceous/non-siliceous mesoporous materials *via* various synthetic approaches. Furthermore, the availability of diverse functionalization methods has been reviewed to provide comprehensive approaches for synthesizing new generations of suitably modified mesoporous materials with superior structural, physicochemical, and textural characteristics.

Received 15th January 2020
Accepted 12th March 2020

DOI: 10.1039/d0ra00440e

rsc.li/rsc-advances

Introduction

Among all synthesized porous materials, microporous zeolites are known as one of the best, with superior characteristics during various processes. The combination of several unique properties, such as ion exchange capabilities, uniform and stable pore structures, and good thermal and mechanical stabilities, gives them the potential to be widely applied to separation, sorption, catalysis, *etc.* Over the last few decades, several innovative fabrication methodologies have been applied to enhance the structural and textural characteristics of these zeolites. However, some limitations, such as weaker acid strength and less functionalization capabilities (due to small pore sizes), have encouraged the scientific community to design and synthesize alternative advanced materials. Following the invention of the very first generation of ordered mesoporous silica (OMS) materials, tremendous attention has been paid to the development of new compositions and structures through the synthesis of silica/non-silica mesoporous materials.

Recently, diverse synthetic approaches have been proposed for fabricating inorganic mesoporous materials. According to empirical studies, there are several key synthesis approaches and parameters that can affect the structural and morphological characteristics of the final materials, including the properties of the components, chemical ratios, operating times and temperatures, pH values, and type of reactor used (reflux system, or microwave or autoclave assisted techniques). Generally speaking, the synthesis of mesostructured materials can be controlled through altering the surfactant type (ionic or non-ionic) and the interaction mechanism between the template (if employed) and silica components.[1,2] M41S silica molecular sieves were initially synthesized under alkaline conditions, where the anionic inorganic species (I^-) become stable in the presence of the cationic surfactant (S^+) through S^+I^- strong interactions. Similarly, silica mesostructures could be shaped with an anionic surfactant (S^-) under acidic

[a]*Department of Chemical and Environmental Engineering, Universiti Putra Malaysia, 43400 Selangor, Malaysia. E-mail: soroush.soltaani@gmail.com; Tel: +60 122635051*
[b]*Department of Physics, Islamic Azad University, Karaj, Iran*
[c]*Institute of Advanced Technology, Universiti Putra Malaysia, 43400 Selangor, Malaysia*

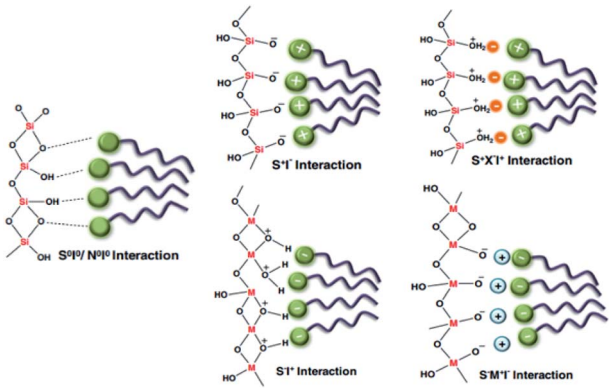

Fig. 1 A schematic illustration showing all types of interaction mechanism between surfactant and silica components[4] [anionic inorganic species: (I^-); cationic inorganic species: (I^+); cationic surfactant: (S^+); anionic surfactant: (S^-)]. Reprinted with permission from ref. 59. Copyright 2011 RSC.

conditions (inorganic species: I^+) using the $S–I^+$ approach. SBA materials are typically synthesized in an acidic environment through a $((S^0H^+)(X^-I^+))$ indirect interaction between the surfactant and positively charged template.[3] Another example is HMS materials, which are formed *via* a (S^0I^0) neutral interaction between an inorganic component and surfactant. All types of interactions are illustrated in Fig. 1.[4] It should be noted that there are other crucial elements, such as the chemical volume, the type of solvent, and the presence of additives (like swelling agents, salts, co-surfactants, and co-solvents), that allow the fine-tuning of the prepared materials.

Generally, the fabrication of templated mesostructured materials can be done through the following steps:

(i) The dissolution of template components in the solvent.

(ii) The addition of the silica source under constant stirring.

(iii) Hydrolysis and pre-condensation at a certain reaction temperature using appropriate thermal treatment.

(iv) The recovery of the as-synthesized sample through washing and drying treatments.

(v) The removal of the template using either extraction or calcination techniques.

The extraction approach often remains incomplete and cannot be applied to all surfactants and sources.[5] However, it is preferred from cost-effective and environmental perspectives as it allows for the recovery or reuse of templates. The calcination procedure leads to the further condensation of the silica matrix in contrast to the extraction approach. A schematic overview of the soft templating approach *via* two synthetic methodologies, (a) cooperative self-assembly and (b) a "true" liquid-crystal templating process, for the fabrication of ordered mesoporous materials is demonstrated in Fig. 2.[6] During the cooperative self-assembly procedure, inorganic components interact with surfactants motivated by coulombic forces, hydrogen bonding or covalent bonds. At the interface, the inorganic components polymerize and crosslink, and subsequently cooperatively assemble with the surfactants. Throughout the reaction, supportive charge density and surfactant arrangements between the organic and inorganic components affect each other. Therefore, the compositions of organic–inorganic hybrids are different to some degree. Similar charge densities are arranged at the surfactant/inorganic interfaces during the assembly procedure, accordingly resulting in phase separation and restructuring, and finally leading to the development of an ordered three-dimensional structure with the lowest energy. On the other hand, the "true" liquid-crystal templating process is based on true or semi-liquid-crystal mesophase micelles, which are produced using high-concentration surfactants as templates. The condensation of inorganic precursors is enhanced due to restrained growth around the surfactants,

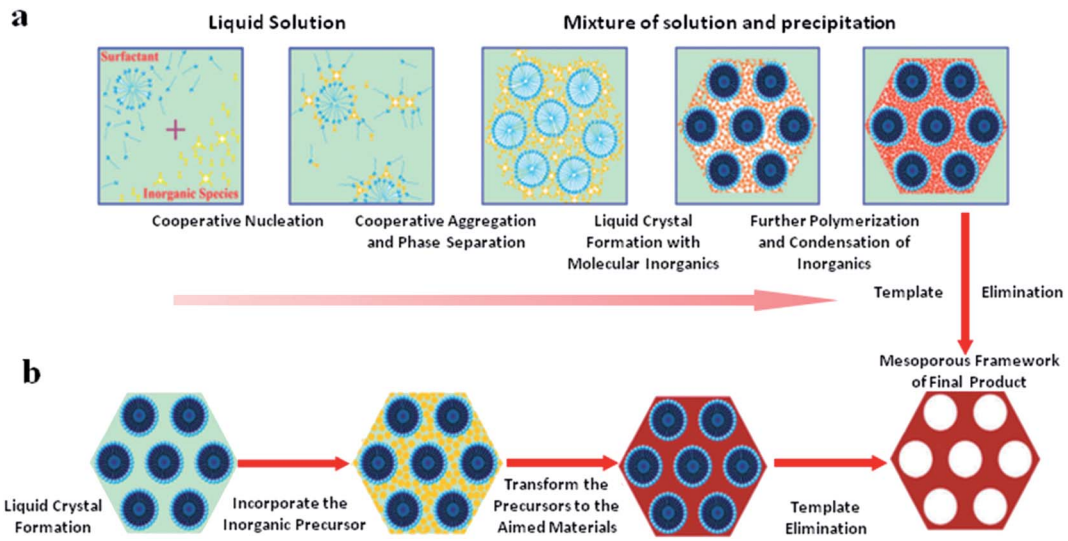

Fig. 2 A schematic overview of the soft templating approach *via* two synthetic methodologies, (a) cooperative self-assembly and (b) "true" liquid-crystal templating processes, for the fabrication of ordered mesoporous materials,[6] modified fromref. 7. Reprinted with permission from ref. 6 and 7. Copyright 2013 RSC.

leading to the structuring of ceramic-like frameworks. Straight after condensation, the organic templates can be detached.

For the synthesis of non-siliceous mesoporous materials, despite the highlighted important elements, the rates of hydrolysis and condensation play crucial roles in controlling the formation of the structure. This is because of the fact that the hydrolysis and condensation processes happen more rapidly for transition metal oxides in comparison with silica materials. So far, comprehensive research has been conducted to allow for the good control of the hydrolysis and condensation processes to avoid phase separations. Indeed, suitable interactions between the surfactant and inorganic components are the result of controlled hydrolysis and condensation procedures. This can occur through increasing the solubility of the metal oxides by adjusting the pH and controlling the amount of water to restrict hydrolysis.[8–10] An important point that needs to be taken into consideration is that the thermal stabilities of transition metal oxides are low because of crystallization, phase transitions, and redox reactions. However, there are strategies, such as the extraction of the surfactant as an alternative to calcination, to eliminate unwanted crystallization and avoid structural collapse upon the functionalization of these materials. On the other hand, calcination procedures can be conducted when high crystallinity is a matter of importance. Through the synthesis of mesoporous transition metal oxides, functionalization treatments can be carried out to modify the structural stability.

In the current paper, a brief comparison of zeolites with mesoporous materials has been provided. Attempts have been made to provide an overview of some of the most favourable approaches for the synthesis of siliceous/non-siliceous mesostructured materials. In order to modify siliceous/non-siliceous mesoporous materials, it is highly essential to bridge the knowledge gap between the structure of the materials and their functionality for desired applications. Furthermore, numerous synthetic schemes relating to functionalization are reviewed that allow for better control through the incorporation and, importantly, distribution of functional components within the mesostructured matrix. From this viewpoint, several highly cited papers have been published in this area; these are undoubtedly landmarks and historical contributions when it comes to the development of ordered mesoporous materials and the evolution of this field since its discovery, and progress has been based on these achievements.[7,11–16] The authors do not propose that this is the only promising material relating to mesoporous composites, but the key purpose is to stimulate further research into mesoporous materials and to formulate new synthetic procedures and functionalization steps for a wide range of applications.

Mesostructured materials *versus* zeolites

The discovery of porous materials, particularly zeolites, has generated significant environmental and economic advantages over various other industrial developments. The actual portfolio of microporous architectures, including 201 framework forms, 22 disordered zeolite frameworks and several unknown structures, has been officially recognized by the Structure Commission of the International Zeolite Association.[13] Despite the huge variety of zeolite structures, pore diameter has remained a main barrier to chemical reactions involving bulky particles. Therefore, the development of mesoporous materials with pore sizes ranging from 2–50 nm would be a proper answer to this problem. The discovery of ordered mesoporous materials goes back 20 years to the scientists of Mobil;[17] this attracted the attention of the scientific community, who were aware of the remarkable characteristics of these mesostructured materials.

From a physicochemical point of view, mesoporous materials cannot be distinguished from zeolites, however, these materials should be strictly linked to microstructured materials. The fabrication of mesoporous materials can be considered as a development from zeolites. In the process of the crystallization of microporous materials, organic molecules, which are called templates, hydrate inorganic cations to form three dimensional zeolite architectures. Then, template removal takes place based on chemical extraction or calcination to form microstructures with pore sizes of less than 1 nm. In the case of mesoporous materials, amphiphilic surfactant molecules of various natures (cationic, anionic, non-ionic) containing a hydrophilic polar head play a crucial role in the formation of micelles with different shapes (such as bi-layers, spheres or rods) in the presence of a polar medium.[18] The shape of the micelles can be varied by varying the ratio of surfactant molecules to polar chains. It should be noted that the final product possesses the real shape and diameter of the mesoporous architecture.

On the other hand, the low thermal or hydrothermal stabilities and acid strengths of mesostructured materials are still the main barriers preventing their industrial application in comparison with zeolites. Generally speaking, the lack of these properties is related to their amorphous natures. However, these critical issues can be eliminated through various post-functionalization treatments. These can be performed using metal and non-metal elements in the reaction mixture, resulting in the homogeneous dispersal of heteroatoms. In this approach, acid strength can be controlled through the incorporation of monomeric species of Al, such as $NaAlO_2$, $Al(i\text{-}PrO)_3$ and $Al_2(SO_4)_3$, into the amorphous walls, however, dealumination may be enhanced by reducing the SiO_2/Al_2O_3 molar ratio.[19,20]

Nevertheless, a removal process involving calcination or ion exchange may lead to the formation of both Lewis and Brønsted acid types; however, these Brønsted sites are not comparable with those present in zeolite structures in terms of strength. The acid strengths of mesostructured materials were examined *via* the pyridine adsorption–desorption technique using Fourier-transform infrared spectroscopy (FTIR). According to the data reported in Table 1, zeolite beta contains the highest concentration of both Lewis and Brønsted acid sites compared with mesoporous silica alumina (MSA), amorphous microporous silica-alumina (ERS-8), and MCM-41.[21]

Table 1 The type, strength and number of acid sites present in materials used for the isopropylation of toluene.[21] Reprinted with permission from ref. 21. Copyright 1999 Elsevier

Acid strength (μmol g^{-1})							
		Weak		Medium		Strong	
Material	Si/Al	Lewis	Brønsted	Lewis	Brønsted	Lewis	Brønsted
Zeolite beta	11	117	86	12	69	211	125
MCM-41	19	45	83	41	20	87	17
MSA	50	17	23	7	14	77	10
ERS-8	50	15	21	20	17	73	0

The innovation of mesoporous materials has led to new research interest in employing nanosized mesoporous materials, due to their possession of remarkable physical properties for a wide range of prospective applications in different industrial fields. These nanoparticular matrices could have high loading capacities and good mass-transfer characteristics because of their extremely large surface areas and flexible and tunable pore structures. The mesoporous structure can be controlled *via* the sophisticated selection of surfactants or templates. Besides, the pore size can also be controlled by varying the reaction parameters (such as the chemical composition and operating temperature) or adding supporting organic chemicals. Up to know, only a few elements (such as Ge, V, Ti, Fe, B, and Ga) can be accommodated into zeolites, while many more elements (such as Sn, Zr, Ta, Nb, Zn, *etc.*) can be incorporated into meso-frameworks. Moreover, nanoscale mixed metal oxides can form in the mesopore walls, which is highly impossible in the case of zeolites due to pore diameter limitations.

The surface areas and porosities of synthesized samples can be controlled through varying the calcination temperature. During the post-annealing process, typically the template condenses on a large scale, which leads to the formation of larger pore diameters.[22,23]

Summary of key mesostructured materials

Silica-based mesoporous materials

Siliceous mesoporous materials are recent developments in the field of nanotechnology, possessing mesoporous silica architecture. The most common classes of mesostructured materials are Mobil Composition of Matter (or Mobil Crystalline Materials, MCM) and Santa Barbara Amorphous (SBA). The very first generation of mesostructured silica was synthesized in 1970 and went almost unnoticed. Research continued into mesoporous architectures and, later, MCM was fabricated at Mobil Corporation laboratories. Six years later, researchers at the University of California, Santa Barbara successfully synthesized mesostructured silica nanoparticles (MSNs) with hexagonal arrays of pores possessing much larger pore diameters, ranging from 4 nm to 30 nm; this was named SBA-15.

The very first reported silica mesophase material was M41S, which is known as an MCM and is in the mesoporous range. It was initially synthesized by Mobil researchers in 1992 through self-assembly with a surfactant as a template to form SiO_2 mesoporous materials. M41S materials possess uniform and long-range porosity with pore walls of amorphous silica. M41S materials can be classified into three major types: MCM-41 (cubic); MCM-48 (hexagonal); and MCM-50 (rod).[10] There are several key factors that greatly influence the formation of M41S materials, such as the kind of surfactant and its chain length, the operating temperature and operating time, the hydrogel structure, and the alkalinity. The mesophase class can be verified *via* measuring the surfactant packing factor (*g* factor, see eqn (1) and Fig. 3(a)), which also describes the hydrophobicity and hydrophilicity of the materials:

$$g = \frac{V}{la_o} \quad (1)$$

where V is the total volume of the surfactant plus any other additives among the chains, l is the length of the kinetic

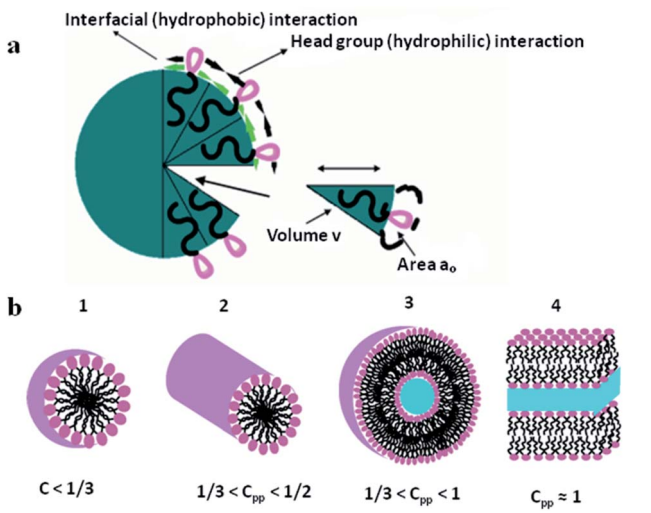

Fig. 3 (a) A schematic illustration of surfactant self-assembly demonstrating the critical packing parameters[24] and (b) the critical packing factors based on head group area, total volume and the length of the surfactant tail.[25] Reprinted with permission from ref. 24 and 25. Copyright 2011 and 2016 respectively MDPI.

surfactant tail, and a_o is the operative head group area at the surface of the micelles.

From a classical micelle chemistry point of view, a mesostructure can be formed only if the *g* value goes above a critical value. In this regard, spherical architecture can be obtained in the presence of polar head groups with large surface area, and a rod structure can occur due to the tight aggregation of polar head groups. However, by changing the *g* factor using different reaction conditions, the ordering of the materials will be affected (see Fig. 3(b)). In general, for packing factors of 1/3, 1/2, 1/2–2/3, and 1, the mesophase can involve cubic (*Pm3n*), hexagonal (*P6m*), cubic (*la3d*), and rod structures, respectively.

MCM-41. MCM-41 is one of the most examined kinds of M41S material, consisting of amorphous silicate architecture and uniform hexagonal pores. The uniformity is the reason for the distribution of narrow pores and pore walls, where the pores are arranged unidirectionally in a honeycomb architecture.[26,27] Fig. 4 depicts a schematic illustration of the hexagonally shaped MCM-41.[28]

For conventional MCM-41 materials, the pore diameters vary between 1.5 and 20 nm, where larger pore diameters can be formed in the presence of an excess amount of swelling agent. The occurrence of narrow pore walls in the MCM-41 architecture is the main reason for its low thermal, hydrothermal, and chemical stabilities.[29,30] However, attempts have been made to maximize the stability of this material either *via* the *in situ* doping of numerous salts or post-functionalization treatments.[16]

MCM-48. Ordered MCM-48 is another kind of M41S material, which is typically synthesized with surfactant : silica ratios greater than 1. Cubic MCM-48 material possesses similar textural properties to MCM-41; it also has narrow pore walls, leading to similar limitations. A notable structural characteristic of the MCM-48 material is its three-dimensional bicontinuous pore structure.[31] In comparison with one-dimensional systems, the three-dimensional network brings about several advantages relating to separation and catalysis systems, significantly reducing diffusion limitations.

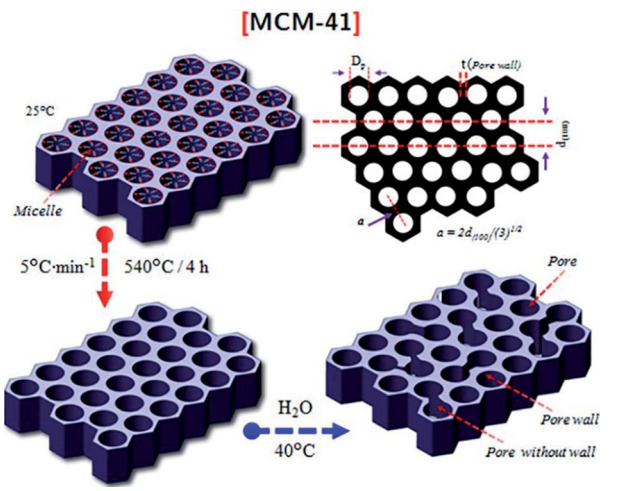

Fig. 4 A schematic illustration of the hexagonally shaped MCM-41.[28] Reprinted with permission from ref. 28. Copyright 2019 Elsevier.

SBA materials. SBA materials are another class of highly ordered mesoporous silica material, which were initially synthesized and reported in an acid medium using triblock copolymers ($EO_nPO_mEO_n$) in 1998. So far, a wide diversity of SBA materials has been prepared and reported, consisting of cubic SBA-1, cubic SBA-11, three-dimensional hexagonal network SBA-12, lamellar SBA-14, two-dimensional hexagonal SBA-15, and cubic cage-structured SBA-16. Among the SBA family, SBA-15 and SBA-16 have attracted great attention due to their remarkable structures and characteristics.[32]

SBA-15. SBA-15 is considered a combined micro/mesoporous material, and its porosity highly depends on the synthesis conditions. It possesses a hexagonal framework with tuneable uniform mesopores and thick microporous pore walls of 3–6 nm. The combination of these features enhances the hydrothermal and chemical stabilities of SBA-15 in comparison with M41S material.[33] It has been reported that SBA-15 possesses pores with a curved nature, which enhances the adsorption capacity as molecules can easily diffuse into the framework.[34] Functionalized mesoporous SBA-15 was fabricated by Sajad *et al.*[35] using a co-condensation method. The pore structure of the synthesized SBA-15 was characterized *via* high resolution transmission electron microscopy (HR-TEM), as shown in Fig. 5. The top view surface TEM images show a honeycomb-like

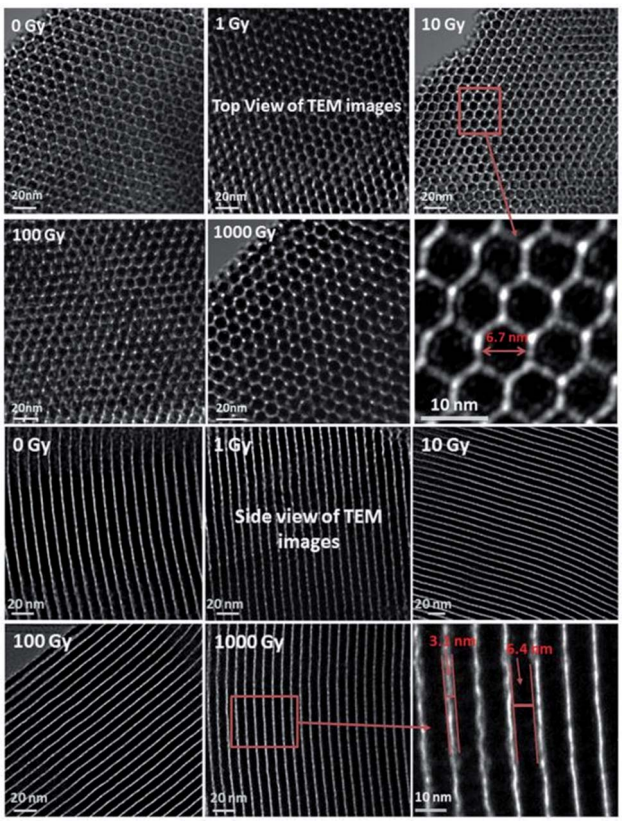

Fig. 5 HRTEM images of SBA-15 from the top, with the honeycomb-like mesoporous morphology formation visible, and the side, with the highly parallel, homogeneous pores and channel-like structure visible. Reprinted with permission from ref. 35. Copyright 2018 ACS Nano.

mesoporous structural morphology with high uniformity and an average diameter of around 6.5 nm in the absence of any pore widening (as seen in the magnified image in Fig. 5). The side view morphology of SBA-15 demonstrates an extremely parallel and homogeneous channel-like structure. The typical wall thickness of SBA-15 was around 3 nm; however, the average width of the channels was around 6.7 nm.

It is worth mentioning that SBA-15 possesses a highly stable internal architecture of mesopores due to its highly hydrophobic nature.[36] Through varying the lengths of the copolymer blocks, the internal stability and pore wall thickness can be tuned.[37] However, there are other parameters that directly or indirectly affect the morphologies and general characteristics of SBA-15 materials, such as the operating temperature, pH value, and kind of additives used (like salts, co-surfactants, and swelling agents). Up to now, a large variety of morphologies have been reported for SBA-15, consisting of platelets, spheres, and rods. Fig. 6 displays scanning electron microscopy (SEM) images of a few SBA-15 morphologies. Moreover, due to their desirable characteristics, SBA-15 materials have high potential to be introduced as templates for the fabrication of carbon replicates and nanowires using different metals.[38]

SBA-16. SBA-16 is typically formed when block copolymers with longer EO chains are applied (as templates) at room temperature under acidic conditions. The presence of large EO chains brings about the fabrication of spherical structures.[40] Similar to SBA-15, the template can be further eliminated through either post-calcination or extraction in the presence of ethanol. By removing the template, a material with a micro/mesoporous structure is obtained. It should be noted that the

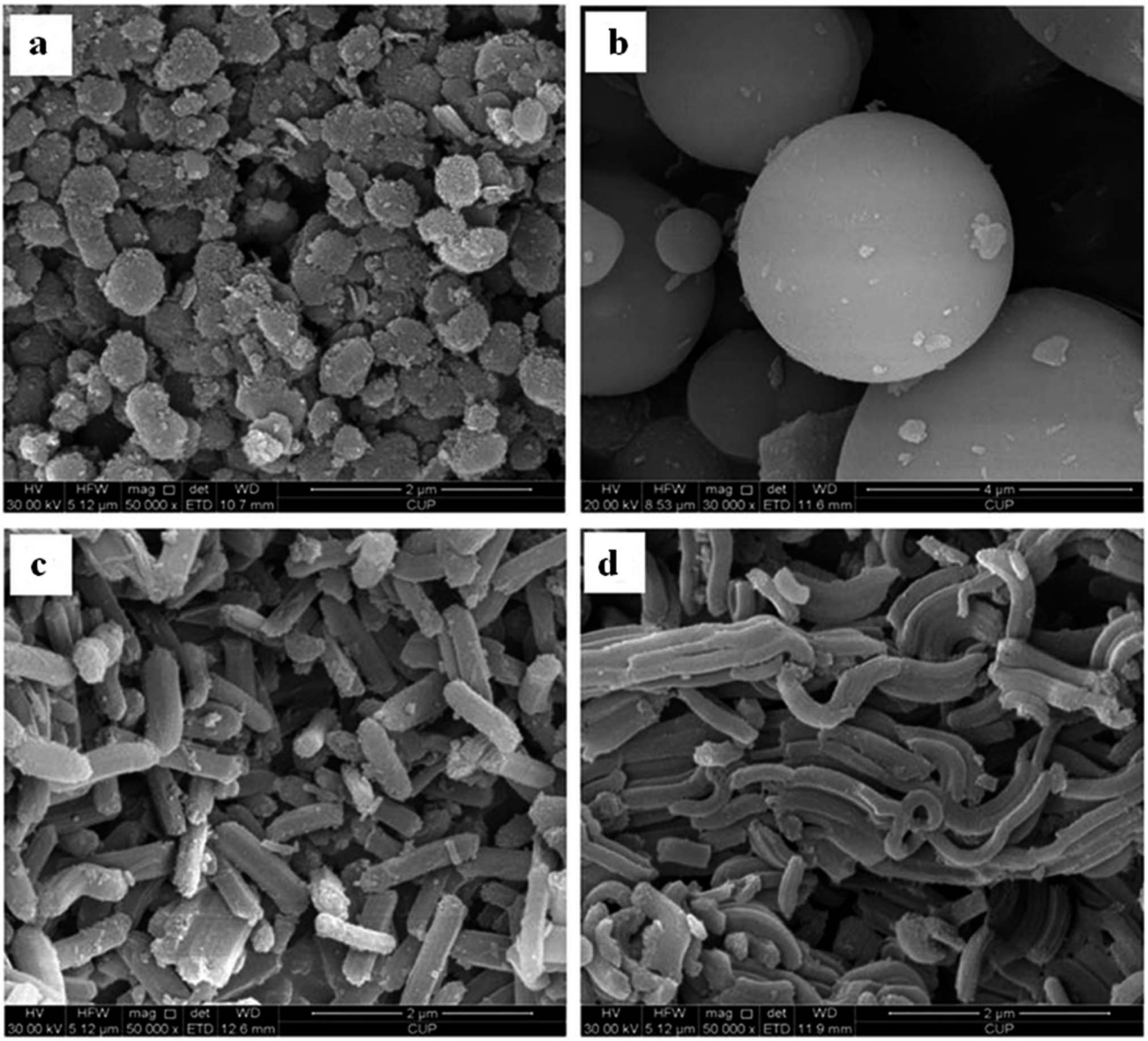

Fig. 6 SEM images displaying examples of a few morphologies of SBA-15: platelets (a); spheres (b); short-rods (c); and long-rods (d).[39] Reprinted with permission from ref. 39. Copyright 2015 RSC.

formation of a combined micro/mesoporous structure is due to the presence of polyethylene oxide (PEO) and polypropylene oxide (PPO) chains, respectively.[41,42] SBA-16 possesses similar textural properties to SBA-15, such as a large surface area, a narrow pore diameter distribution, a pore diameter of 6 nm, and thick pore walls of 4–6 nm. Here, also, the thick pore walls are responsible for the thermal, hydrothermal, and chemical stabilities of SBA-16, which resemble those of SBA-15.[43] Large variations in morphology (cubes, rods, sphere, *etc.*) can be generated *via* varying the synthesis conditions and methods, such as such as the operating temperature, pH value, and doping of some additives.[44] Despite several likenesses with SBA-15, the ordering of the mesopore structure of SBA-16 is different. N_2 sorption isotherms from SBA-16 (hysteresis loop at around $P/P_o = 4.0$) differ from SBA-15 (hysteresis loop at around $P/P_o = 6.0$).[45] Another difference with SBA-15 is that SBA-16 possesses a three-dimensional cubic cage structure, according to its XRD patterns.

SBA-16 materials can be synthesized in powder form or deposited as films on different substrates using inexpensive and eco-friendly systems. The performance of SBA-16 can be highly improved through its functionalization with various organic or hetero-element groups through either *in situ* or post-modification approaches.

Plugged hexagonal templated silica (PHTS). Plugged hexagonal templated silica (PHTS) can be synthesized by raising the ratio of silica to surfactant, and it has similar basic properties to SBA-15.[46] As an ordered mesoporous material, PHTS possesses a uniform hexagonal combined micro/mesoporous structure with a pore diameter, pore volume, and pore wall thickness similar to SBA-15 materials.[47] Fig. 7 illustrates the N_2 sorption isotherm of a typical PHTS material. The following characteristics can be observed: (i) adsorption in the intrawall micropores at a low relative pressures; (ii) multi-layer adsorption in the regular mesopores and the concentration of capillaries in the narrow intrawall mesopores; (iii) single-step capillary condensation, representing homogeneous mesopores; and (iv) dual-step desorption subdivision, representing the pore blocking effects at a relative pressure of 0.45. It should be mentioned that the microporosity of the plug may be increased by increasing the operating temperature. The hydrothermal stability of PHTS is remarkably high, and it can be improved even further through higher operating temperatures and operating times.[43] Due to its high hydrothermal stability, PHTS is highly suitable for various catalytic applications.

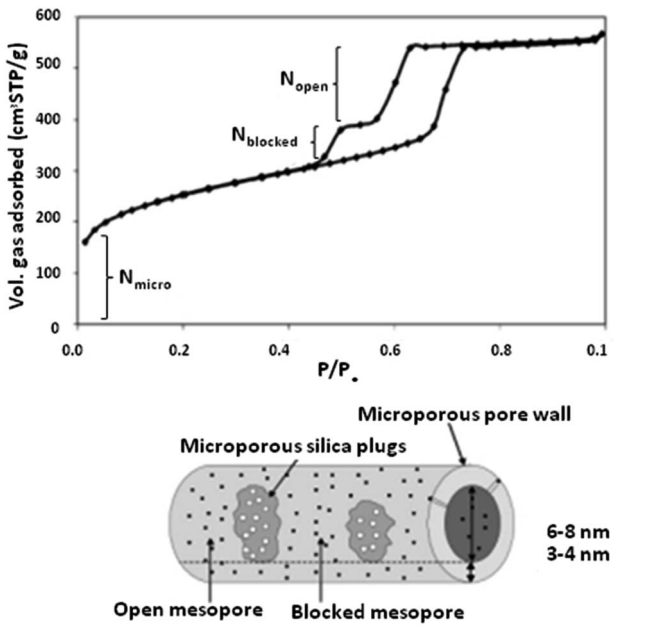

Fig. 7 An N_2 sorption isotherm of a typical PHTS material.[48] Reprinted with permission from ref. 48. Copyright 2002 RSC.

To date, various morphologies of PHTS are known and have been reported. According to the literature, different morphologies can be shaped *via* tuning the stirring temperature and concentration of tetraethylorthosilicate (TEOS) used in the synthesis procedure. For instance, a high stirring temperature leads to the formation of spherical morphology, while low TEOS amounts and stirring temperatures lead to smooth rods.[49,50]

The functionalization of PHTS can be performed *via* introducing catalytically active elements. In this procedure, metal particles can be dispersed on the surface of PHTS using different methods (such as molecular designed dispersion (MDD)), followed by post-calcination. By cautiously choosing the right method, and tuning the size of the nanoparticles and the applied temperature, the active elements can be selectively positioned either (i) in the plugged sections, (ii) in the pores, (iii) on the surfaces of open pores, or (iv) in the silica walls.

Mesostructured cellular foam (MCF). Mesostructured cellular foam (MCF) is typically synthesized in the presence of a proper swelling agent, like mesitylene (1,3,5-trimethylbenzene), to fabricate SBA-15 as a monolith or bulk powder.[51] The reason for using a swelling agent is to enlarge the micelles and form a sponge-like foam. MCF materials possess unique three-dimensional structural features, with large and uniform spherical cells in the range of 15–50 nm and large windows (see Fig. 8(a, c, and d)). The high hydrothermal stabilities of these materials are confirmed based on their thick and uniform pore walls. The N_2 sorption isotherm of MCF illustrates the presence of an inkbottle-type mesostructure, as fairly large and uniform cells are interconnected by windows, maximizing the approachability of the spherical cells (Fig. 8(b)).

The structural characteristics, morphologies and particle sizes of MCF can be controlled through adjusting the synthesis conditions and methods, such as the operating temperature, pH value, and doping of some additives.[52–54] The functionalization of MCF materials can be performed using either *in situ* or post-modification methods to enhance their capabilities.[55] Having a larger pore structure increases mass transfer and also increases the chances of large molecules accessing the mesopore channels, which is beneficial for various applications, such as separation, sorption, catalysis, *etc.*

MSU. The abbreviation MSU stands for Michigan State University, where the fabrication of MSU took place. MSU materials are synthesized in neutral (non-acidic) media in the presence of non-ionic polyethylene glycol (PEG) polymers as films, powders, and monoliths.[57,58] It should be noted that the

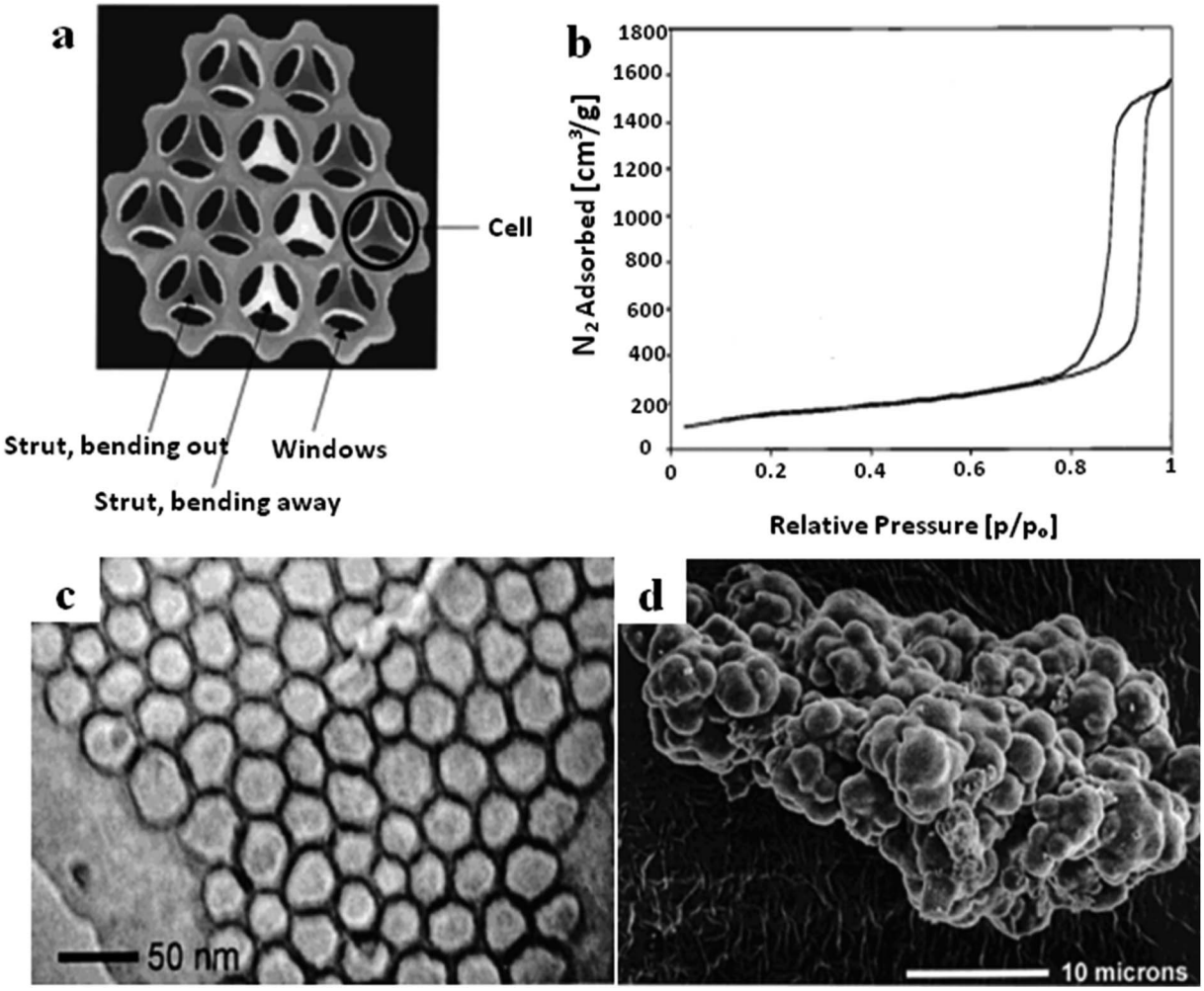

Fig. 8 (a) A schematic cross-section diagram of the strut-like structure of MCF. (b) The N_2 sorption isotherm of MCF. (c) A TEM image of MCF at high magnification. (d) An SEM image of MCF with cauliflower-type morphology.[56] Reprinted with permission from ref. 56. Copyright 2000 American Chemical Society.

introduction of tri-block polymers is unnecessary for templating purposes. Typically, MSU materials are named as MSU-*X* (such as MSU-1, MSU-2, MSU-3, MSU-4, MSU-F, MSU-S, and MSU-V), where the letter *X* is used to differentiate various families of materials. A majority of MSU materials possesses a wormhole framework with a highly ordered mesophase. Fig. 9 shows TEM images of synthesized silica core–shell nanoparticles with an MSU shell in the presence of different non-ionic PEO surfactants based on a two-step sol–gel technique.[59] The images display the typical wormhole pore frameworks of all the samples.

Because of the fact that the synthesis process takes place in a neutral (non-acidic) medium, there is neutral contact between the inorganic material and surfactant of the type S^0I^0, which significantly eases the separation of the surfactant. In this regard, the synthesis process can be done in a more cost-effective manner due to the greater recycling yield of the surfactant after the separation step. Similar to all mesoporous templated materials, the morphological and structural features of MSU could be adjusted *via* tuning the synthesis conditions and methods, such as the operating temperature, pH value, and doping of some additives.[60–62]

Direct liquid crystal templating (DLCT). Direct liquid crystal templating (DLCT) is another approach to synthesize mesostructured materials in the super-micro/mesoporous range using both non-ionic and ionic surfactants.[63] Using this solvent-free synthesis route, a high concentration of surfactant (greater than 20 wt%) is required in the presence of hydrophilic domains compared to sol–gel methods. The sizes and morphologies of the macroscopic (monolithic) pores can be adjusted and no ion-exchange step is required (due to the absence of cations).

The DLCT procedure can be used for the fabrication of mesostructured silica and aluminosilicates. Alkylene oxide segments present in the surfactant interact with inorganic ions, resulting in the direct formation of mesoporous silica. This interaction allows for the smooth diffusion of heteroatoms through the silica framework. According to reports, as well as aluminum, noble and base metal ions (such as Pt, Ru, Rh, Ni,

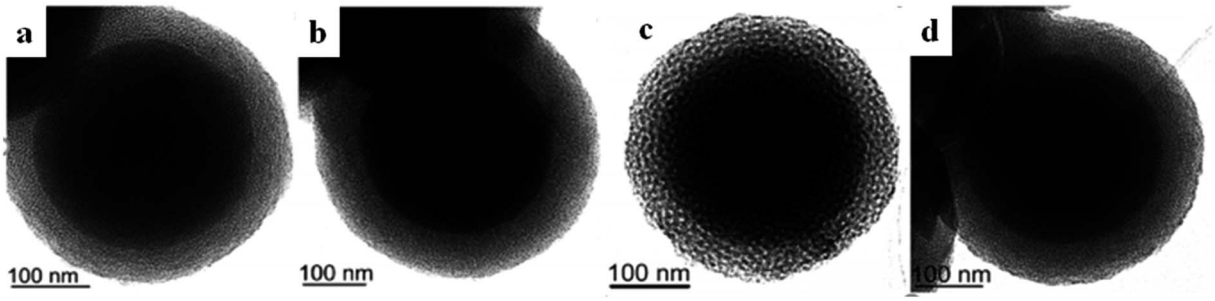

Fig. 9 (a–d) TEM micrographs of MSU-1, MSU-2, MSU-3, and MSU-4, respectively, with noticeable core–shell structures and mesoporous shells, as evidently highlighted by the higher contrast of the core.[59] Reprinted with permission from ref. 59. Copyright 2011 RSC.

Co, Ag, and Cu) can be incorporated into mesostructured silica and aluminosilicates.[64–68]

It is worth mentioning that the characteristics, especially the acid strengths of the sites, of DLCT aluminosilicates highly depend on the Si : Al ratio, however, the acid strengths at all Si : Al ratios are greater than in MCM-41 materials. This characteristic is a matter of interest in catalysis, where a requirement is the presence of medium acid strength.

Non-silica based mesoporous materials

Surfactant templating methodologies have been used to synthesize non-silica based mesostructured materials since 1993. To date, several species of non-siliceous mesostructured solids have become known, consisting of metal oxide, phosphate, and sulphide based materials.[69] Non-siliceous mesostructured materials are synthesized under a large range of reaction conditions in the presence of surfactants of different natures (ionic, cationic, geminal, or neutral). These materials possess unique characteristics, including tolerating diverse fabrication conditions, and having pore diameter (ranging from 2 nm to 10 nm) and framework structure flexibility, making them applicable to various application fields. It has been stated that the oxidation states of transition metal ions have a great impact on composite mesoporous materials.[70,71]

Templated mesoporous transition metal oxides. Templated mesostructured transition metal oxides (TMOs) are another category of synthesized mesoporous materials. However, the reactivity of transition metal sources is high compared with silica sources. The formation of mesostructured materials can take place upon carefully controlling the reaction conditions, including factors such as hydrolysis and condensation. It should be considered that very high reactivity may cause uncontrollable phase transformations and redux reactions. For instance, due to quick hydrolysis and condensation reactions, some transition metal oxides, like titania, show non-porous features. Among the diverse approaches used to fabricate mesoporous titania, evaporation-induced self-assembly (EISA) is known to be a promising method to lower reactivity (due to the presence of non-aqueous solvents like ethanol) and eliminate condensation (due to the presence of acidic inhibition). According to experimental results, mixing two forms of titania sources leads to the formation of highly ordered mesoporous materials. For instance, mixing alkaline titanium alkoxide and acidic titanium salt ($TiCl_4$) brings about the low-degree polymerization of the homogeneous precursors and the self-disciplined polymerization of the inorganic components.

One-dimensional mesoporous anatase TiO_2 nanocrystals were fabricated using carbon nanotubes (CNTs) as a pore-forming agent.[72] The synthesized mesoporous TiO_2 possessed nanoscale and sub-microscale components with a large surface area of 102.1 $m^2\ g^{-1}$ and a pore diameter of 12 nm. In other research, Du *et al.* synthesized two-dimensional hexagonal (*p6mm*) ordered mesoporous TiO_2 using colloidal crystals as a pore-forming agent.[73] The synthesized ordered mesoporous TiO_2 possessed unified periodic macropore channels and a large specific surface area and pore diameter of 256 $m^2\ g^{-1}$ and 4.9 nm, respectively. As shown in Fig. 10, the existence of unified periodic macropores reduced the length of the mesoporous matrix and improved the specific surface area of the

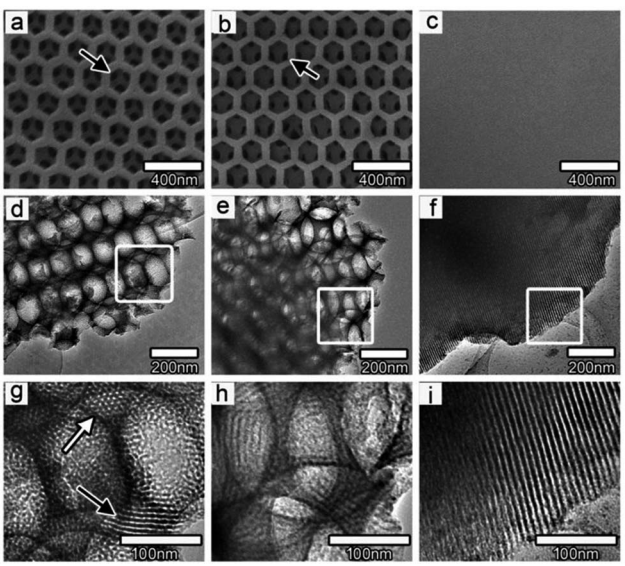

Fig. 10 TEM and SEM images of (a, d, g) macro-mesoporous TiO_2 film, (b, e, h) TiO_2 film with graphene, and (c, f, i) pure mesoporous TiO_2 film. (a, b) The black arrows point out the unified channels between the macropores in the film, while (g) the white and black arrows indicate the mesopores contained in the macropore walls.[73] Reprinted with permission from ref. 73. Copyright 2011 American Chemical Society.

synthesized material. Furthermore, graphene was also added to the ordered macro-mesoporous TiO_2 structure to avoid the recombination of charge in the film because of its exceptional electrical characteristics. In other research, Lin Chen *et al.*[74] utilized $TiCl_4$ and $Ti(OBu)_4$ as titania resources in the presence of P123 as a template to fabricate three-dimensional mesoporous titanium dioxide using the EISA method.

With the EISA technique, micelles are formed through solvent evaporation, followed by hydrolysis and condensation to provide strong interactions between the template and inorganic titania.[75] As the framework is formed, such a slight thermal procedure will play a role in strengthening the network followed by template extraction *via* post-calcination treatment. An important point that needs to be taken into consideration is that uncontrolled thermal and calcination treatments may cause phase transformation and the collapse of the mesostructured framework.[76,77]

Titania materials can be attained in bulk form, as nanoparticles, or as films on various substrate with two-dimensional, three-dimensional, and hierarchical structures.[78] Like mesoporous silica materials, the structural characteristics, morphologies and particle sizes of titania materials can be controlled through adjusting the synthesis conditions and methods, such as the operating temperature, calcination temperature, aging time and pH value.[79] In order to modify the characteristics of mesoporous titania, the functionalization of materials with guest species, like ions, nanoparticles, organic and inorganic molecules, can take place through either *in situ* or post-treatment methods. Fig. 11 displays schematic representations of the synthesis of mesoporous titania films *via* either *in situ* or post-synthesis methods.[80] It has been frequently reported that functionalization through post-synthesis techniques fails to regulate the deposition of foreign particles into the mesostructured framework, resulting in a non-uniform distribution

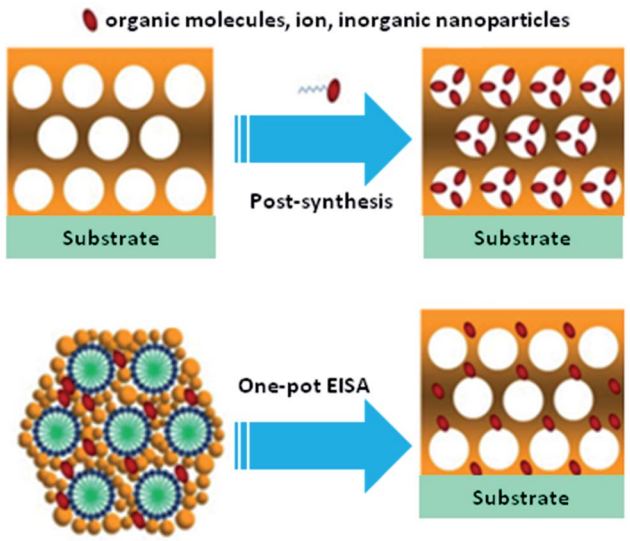

Fig. 11 Schematic representations of the synthesis of mesoporous titania films *via* either *in situ* or post-synthesis methods.[80] Reprinted with permission from ref. 80. Copyright 2011 Elsevier.

in the titania mesoporous material. Moreover, the existence of excess amounts of these particles may block mesopore channels and highly reduce surface areas. The *in situ* method is a promising method, which allows for the high dispersion of guest particles and eliminates crystal growth, the non-uniform distribution of particles, phase transformations, and pore blockages.

Titania nanotubes are another species of TMO material that have received great attention for various applications, such as in electronics, medicine, photocatalysis, catalyst supports, absorbers, sensors, *etc.* Mesostructured titania nanotubes are typically synthesized in the presence of sodium hydroxide using template-free hydrothermal and microwave assisted methods.[81–84] These materials possess open-ended pores, easing the accessibility of reactants to inner pores.

Other than the primary successful route for the fabrication of mesoporous titania, several mesostructured metal oxides and mixed metal oxides have been fabricated *via* hydrogen-bonding, electrostatic mediation, van der Waals, and covalent interactions between template components and metal particles.[85,86] For example, perfect templated zirconium dioxide (ZrO_2) nanodisks were synthesized *via* self-assembly, using $Zr(OC_4H_9)_4$ as a precursor and dodecylbenzenesulfonic acid (DBSA) as a template (see Fig. 12).[87]

In one of our research works, polymeric mesoporous carbon@zinc core–shell spheres were synthesized using a hydrothermal-assisted method in the presence of PEG as the surfactant and D-glucose as the template.[88] In this study, the effects of different zinc concentrations and calcination temperatures on the structural and textural properties of the synthesized samples were examined and are presented in Table 2. The average crystallite size and pore size diameter were increased from 53.26 to 70.36 nm and from 3.45 to 4.63 nm, respectively, upon raising the calcination temperature from 600 °C to 900 °C, however, the specific surface area significantly declined from 396.56 to 174.87 $m^2\ g^{-1}$. It was clearly seen that with an increase in the calcination temperature to 900 °C, the reflection peaks shifted toward higher 2θ angles. This can be attributed to structural shrinkage as a consequence of greater template carbonization. At very high calcination temperatures, D-glucose particles might severely decompose and then collapse, resulting in deformations of the template where ZnO nanoparticles were going to be placed. Furthermore, the shell thickness of the mesoporous carbon@zinc core–shell spheres changed from around 5 nm to 75 nm at different zinc concentrations (2–8 mmol). Similarly, nanocrystalline mesoporous mixed metal oxide (carbon@CuO–ZnO) spheres were hydrothermally fabricated.[89] The effects of different Cu : Zn ratios (0.5, 0.75, and 1.0) on the textural properties were examined; upon raising the metal ratio, the surface area was enhanced (419.13, 477.54, and 517.03 $m^2\ g^{-1}$) while the pore size decreased (3.35, 3.11, and 2.88 nm). In another research work, polymeric mesoporous mixed metal oxides ($ZnAl_2O_4$) with different Al/(Zn + Al) molar ratios (0.5, 0.75, and 1.0) were hydrothermally synthesized.[90] Similarly, upon loading higher metal molar ratios, the surface area increased (414.27–440.38

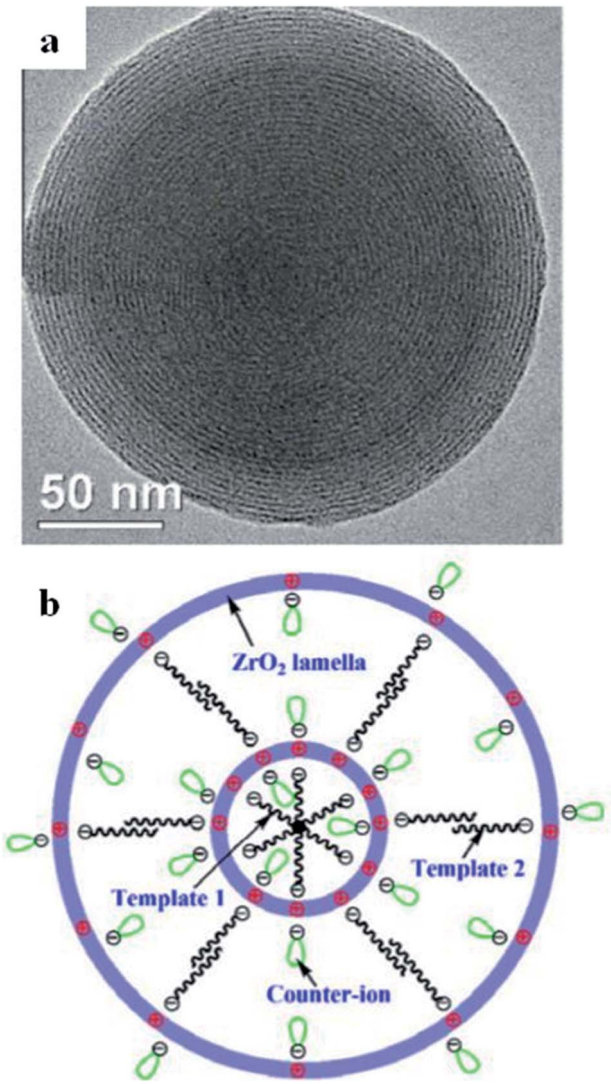

Fig. 12 (a) An ideal DBSA-templated ZrO_2 multi-ring nanodisk self-assembled at 21 °C with Cl^- counter-ions, and (b) the projected structural form of the self-assembled ZrO_2 nanodisks with altered counter-ions.[87] Reprinted with permission from ref. 87. Copyright 2011 Elsevier.

$m^2\ g^{-1}$) while the average pore diameter (3.40–3.10 nm) and average crystallite size (55.92–43.66 nm) decreased.

The strategy for the formation of C@Zn core–shell solids using a PEG-assisted method is displayed in Fig. 13. The formation and development of C@Zn core–shell solid spheres occurred over the following sequence of reaction steps in a Teflon-lined stainless-steel autoclave:[88]

$$n\mathrm{Zn(NO_3)} \rightarrow n\mathrm{Zn^{2+}} + [\mathrm{NO_3}]_{2n} \quad \text{(I)}$$

$$n\mathrm{Zn^{2+}} + \mathrm{OH^-} \rightarrow \mathrm{ZnOH^-} \quad \text{(II)}$$

$$\mathrm{ZnOH^-} \rightarrow \mathrm{ZnOH} + \mathrm{e} \quad \text{(III)}$$

$$\mathrm{ZnOH} + \mathrm{OH^-} \rightarrow \mathrm{Zn(OH)_2} + \mathrm{e} \quad \text{(IV)}$$

$$[\mathrm{Zn(OH)_2}]_n + n\mathrm{PEG} \rightarrow [\mathrm{Zn(OH)_2\text{-}PEG}]_n \quad \text{(V)}$$

Under hydrothermal reaction conditions (high temperature and high pressure), D-glucose, as the carbon source, decomposed into gaseous compounds such as CO, CO_2, and H_2. These compounds further acted as templates for building primary carbon spheres. Along with the formation of carbonaceous spheres, zinc nitrate decomposed to Zn^{2+} cations, which electrostatically interacted with hydrophilic groups (–OH) to form $Zn(OH)_2$ (steps (I)–(III)). As time went by, a complex compound of $[Zn(OH)_2]_n$ formed as neighbouring $Zn(OH)_2$ entities interacted with each other *via* their hydrophilic groups (step (IV)). Next, the oxygen atoms from the PEG components basically adsorbed due to the positive charge of $Zn(OH)_2$ *via* hydrogen bonding to form chains of $[Zn(OH)_2\text{-PEG}]_n$ (step (V)). Basically, PEG molecules were adsorbed on the surfaces of the particles as a result of water-miscible long-range bonding, inhibiting the adhesion and accumulation of metal particles. As the reaction temperature reached 180 °C inside the autoclave, $Zn(OH)_2$ was transformed to zinc oxide (ZnO), which further interacted with and was incorporated into the carbonaceous cores, with a shell of ZnO nanoparticles placed in the exterior layer of the carbon sphere wall. Next, the post-annealing process proceeded to transform the core–shell architecture into a mesostructured one

Table 2 The textural characteristics of mesoporous ZnO nanocrystals synthesized *via* different routes.[88] Reprinted with permission from ref. 88. Copyright 2016 Elsevier

Sample	S_{BET}[a]	Pore diameter[b]	Total pore volume[c]	Average crystallite size[d]
Zinc 2 mmol	126.51	4.60	0.20	60.81
Zinc 4 mmol	216.03	4.56	0.22	57.28
Zinc 6 mmol	345.63	3.52	0.26	53.26
Zinc 8 mmol	290.26	3.91	0.24	49.56
600 °C	396.56	3.45	0.31	53.26
700 °C	345.63	3.52	0.26	57.12
800 °C	209.03	4.59	0.22	60.82
900 °C	174.87	4.63	0.20	70.36

[a] Specific surface areas ($m^2\ g^{-1}$) were obtained using the Brunauer–Emmett–Teller (BET) method. [b] Average pore sizes (nm) were calculated from N_2 desorption branches using the BJH model. [c] Total pore volumes ($cm^3\ g^{-1}$) were calculated at $P/P_o = 0.99$ from the N_2 adsorption isotherms. [d] Average crystallite sizes (nm) were calculated from the value of the FWHM of the (101) diffraction peak using the Scherrer equation.

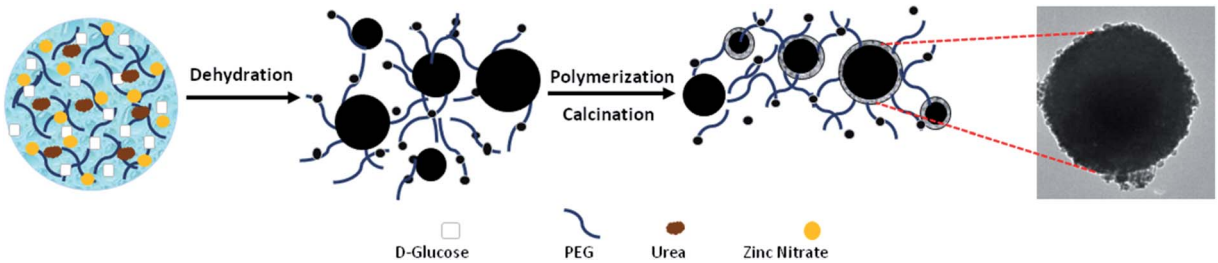

Fig. 13 A schematic representation of the formation of C@Zn using a PEG-assisted method, including an SEM image of a C@Zn solid sphere that was hydrothermally synthesized at 200 °C for 24 h and post-annealed at 600 °C for 4 h.[88] Reprinted with permission from ref. 88. Copyright 2016 Elsevier.

under a N_2 atmosphere; this eventually resulted in the formation of a smooth ZnO shell around a carbon core.

In comparison with silica-based materials, very little attention has been paid to non-silica-based mesostructured composites due to the following reasons:[4]

(i) Transition metal oxides show high reactivity toward hydrolysis and condensation reactions, which results in unrestrained phase separation between inorganic and organic species.

(ii) The crystallization and phase transitions of these oxides often result in a breakdown in structural integrity.

(iii) The synthetic procedures are highly sensitive to some external elements, making it impossible to reproduce results in many cases.

Functionalization of the macroscopic characteristics of mesoporous materials

Functionalization of mesoporous materials can be performed *via* either *in situ* or post-modification methods to enhance their capabilities for the desired applications.

In situ functionalization approaches

The co-condensation of inorganic components. One route to modify the microscopic characteristics of mesoporous materials is to simultaneously incorporate the desired functional components into the mesostructured materials *via* a self-assembly synthesis method. Through a self-assembly synthesis route, either (i) covalent bonds are formed between self-assembling components and functional groups during the co-condensation procedure or (ii) the solubilization of the functional groups take place in self-assembly zones during physical interactions.

The very first advantage of one-pot modification is its simplicity, as the incorporation of functional components into mesopore channels occurs *via* just one synthetic procedure. On the other hand, functional species must only be distributed to the desired regions and must not interrupt the process of mesophase self-assembly. This fact explains some limitations relating to this method in aqueous solutions, as hydrophobic functional components tend to interact with organic templates in the meso-channels, hydrophilic functional components tend to be incorporated into the inorganic framework walls, and amphiphilic functional components tend to be distributed at

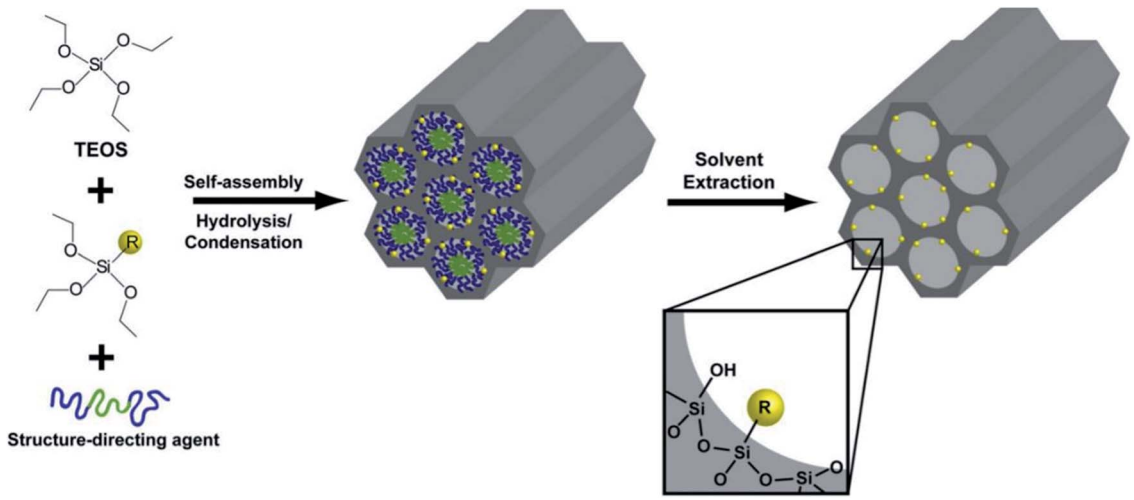

Fig. 14 A schematic representation of a co-condensation method used to incorporate a functional component (R) into mesoporous inorganic materials *via* direct co-assembly.[91] Reprinted with permission from ref. 91. Copyright 2009 Elsevier.

interface sites. Therefore, the choice of functional component plays a crucial role in the choice of one-pot modification route used in an aqueous solution system.

The co-condensation of mixed metal oxides into mesopore channels is a known synthetic route for the functionalization of mesostructured materials. A schematic representation showing a co-condensation method to incorporate a functional component (R) into mesoporous inorganic materials *via* direct co-assembly is illustrated in Fig. 14.[91] The incorporation of Al into mesoporous silica can be taken as an example, as Lewis or Brønsted acid functional components can be incorporated into inorganic meso-channels. Also, the co-condensation of mesoporous silica with transition metal oxides (such as V, Ti, and Cr) and rare-earth elements (such as Tb and Eu) has been widely reported. The solution pH conditions should be chosen according to the template used. For instance, slow precipitation leads to the formation of films, fibers and monoliths, while quick co-condensation leads to the formation of powders. Generally, mesoporous mixed metal oxide materials should be synthesized under basic pH conditions to enable an effective co-condensation procedure with higher heteroatom loading into the silica channels.

Another category of functionalized mesoporous materials is referred to as periodic mesoporous organosilicas (PMOs), which are considered to be innovative organic/inorganic hybrid nanocomposites. PMOs are typically synthesized through hydrolysis and condensation in the presence of organosilica sources using a suitable template and a self-assembly method. As highly ordered mesostructured materials, PMOs possess hexagonal and cubic structures with high surface areas.

Four proposed routes for the fabrication of PMOs with organic species in their frameworks are as follows:[12]

(i) The use of single-bridged organosilica precursors.

(ii) The use of dual bridged organosilica precursors containing diverse functional species.

(iii) The presence of the dangling organic species in the bridged organosilica and silica precursors.

(iv) The post-synthetic functionalization of bridged organic species of the synthesized PMO.

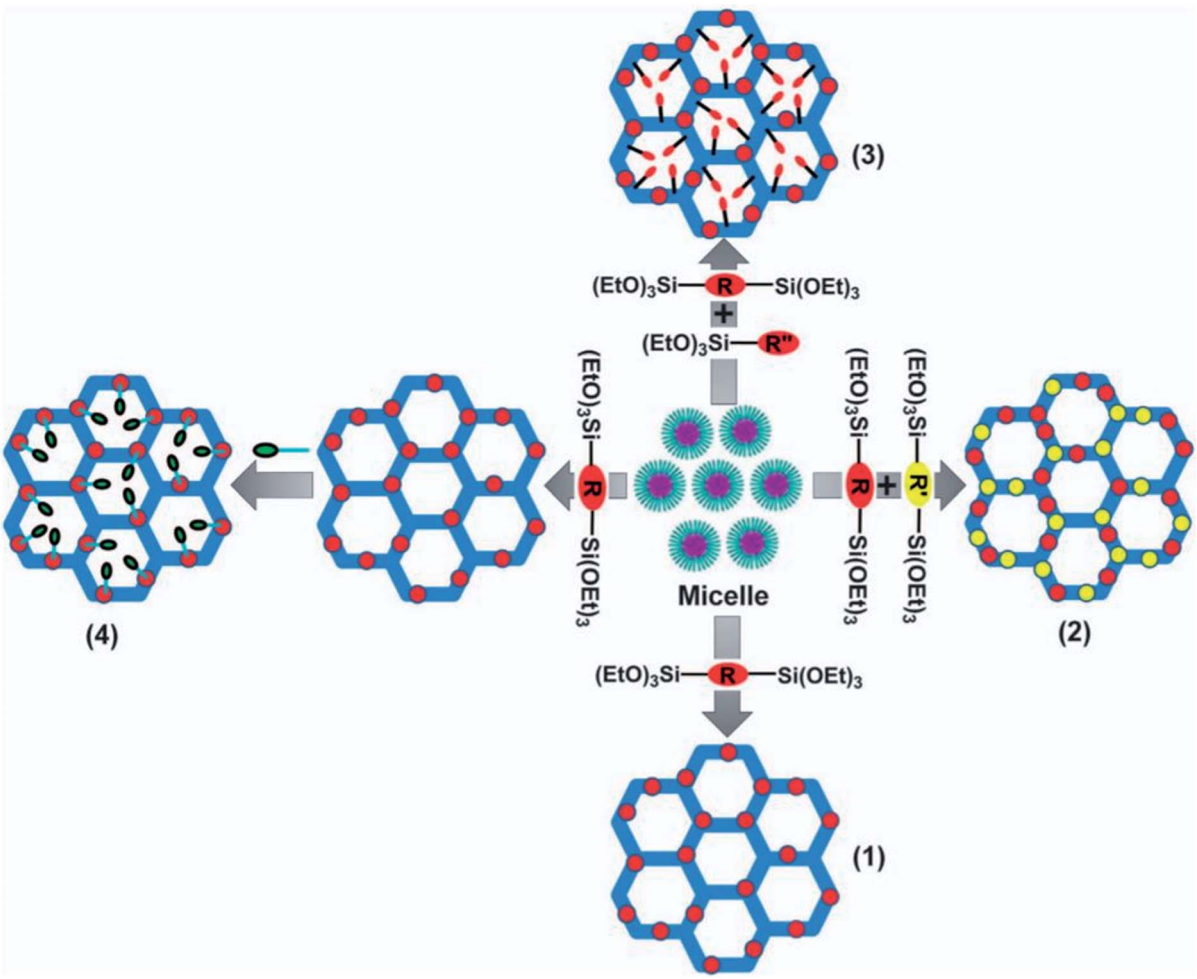

Fig. 15 A schematic representation of the four proposed routes used for the fabrication of PMOs with organic species in their frameworks: (1) a single-bridged organosilica precursor; (2) dual-bridged organosilica precursors with dissimilar functional groups; (3) bridged organosilica and silica precursors with dangling organic groups; and (4) secondary amendment *via* a chemical procedure involving a bridged organic moiety following the fabrication of the PMO.[12] Reprinted with permission from ref. 12. Copyright 2013 Springer Nature.

A schematic representation of the four proposed routes for the fabrication of PMOs with organic species in their frameworks is demonstrated in Fig. 15. The main advantage of PMOs is the uniform hybridization of organic and inorganic components ($(R'O)_3Si\text{-}R\text{-}Si(OR')_3$ (R' = methyl or ethyl; R = the bridged organic groups)) as a bridge within the mesopore walls of silica.[92] Through the organic functionalization of PMO materials, it is possible to highly control surface characteristics such as hydrophobicity and hydrophilicity, and the incorporation of foreign particles. Along with this, there is the inherent potential to protect the mesopore channels from the accumulation of guest particles.[93] In contrast to other siliceous analogs, PMOs possess less fragility and greater hydrophobicity.[94] To date, significant efforts have been made to achieve great advancements in the fabrication of functionalized PMOs for certain applications, such as in gas separation, electronic devices, and catalysis.[12]

Shinji Inagaki *et al.*[95] reported the fabrication of an ordered PMO material, using a benzene-silica hybrid component in the presence of a surfactant. Fig. 16 illustrates a simulated model of the mesoporous benzene-silica with crystal-like pore walls. Benzene chains are arranged in a loop around the pores, associated on two sides with silicate chains, while Si–OH groups are incorporated into silicate at the surface. However, benzene layers with a hydrophobic nature and silicate layers with a hydrophilic nature are arranged along the channels. The orange, red, white, and yellow colours represent silicon, oxygen, carbon, and hydrogen, respectively.

An important point that needs to be taken into consideration is that the hydrophobic/hydrophilic nature and mechanical and chemical properties of these materials can be perfectly tuned *via* the careful arrangement of the framework organic component numbers and species. For instance, the dual surface modification of mesostructured silica can be performed through the self-assembly and co-condensation of acid functional groups and organosiloxane sources using a block co-polymer template. These materials can be used for catalyzing the esterification of free fatty acid (FFA) to produce biodiesel. The hydrophobicity can be improved *via* adding hydrophobic organosiloxane species into the mesopore structure to eradicate the presence of molecules of water near the active sites. It is known that the presence of water causes the formation of soap and deactivates catalysts through chemical reactions.[96–100] In a research work, Yang *et al.*[101,102] applied the one-pot acid functionalization of phenylene-silica *via* co-condensation in the presence of 1,4-bis(triethoxysilyl)benzene and (3-mercaptopropyl)-trimethoxysilane using a non-ionic surfactant in an acidic medium. Characterization proved the successful bonding of oxidized species of the mercaptopropyl group ($C_3H_6SO_3H$) to the silicate mesopore layers (see Fig. 17). The synthesized materials have the great potential to esterify acetic acid in the presence of ethanol.

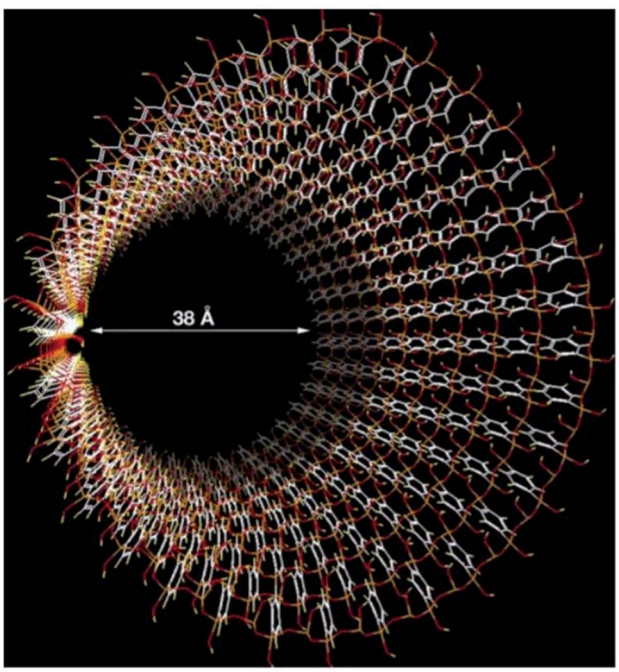

Fig. 16 A simulated model of mesoporous benzene-silica with crystal-like pore walls. Benzene rings are associated in a circle just around the pores, associated on both sides with silicate chains. Silicate was joined to silanol (Si–OH) at the surface. The hydrophilic silicate layers and hydrophobic benzene layers are arrayed alternately at an interval of 7.6 Å along the channel route; silicon: orange; carbon: white; hydrogen: yellow; oxygen: red.[95] Reprinted with permission from ref. 95. Copyright 2002 Springer Nature.

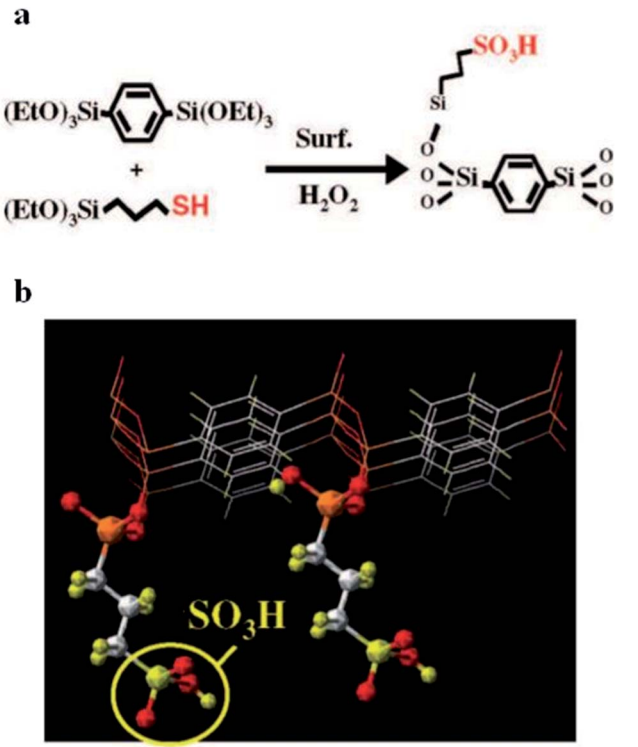

Fig. 17 A schematic illustration indicating (a) the *in situ* fabrication of SO_3H-phenylene-silica *via* co-condensation in the presence of 1,4-bis(triethoxysilyl)benzene and (3-mercaptopropyl)-trimethoxysilane using a non-ionic surfactant in an acidic medium; and (b) a CG image of a functionalized surface with propylsulfonic species.[92] Reprinted with permission from ref. 92. Copyright 2008 American Chemical Society.

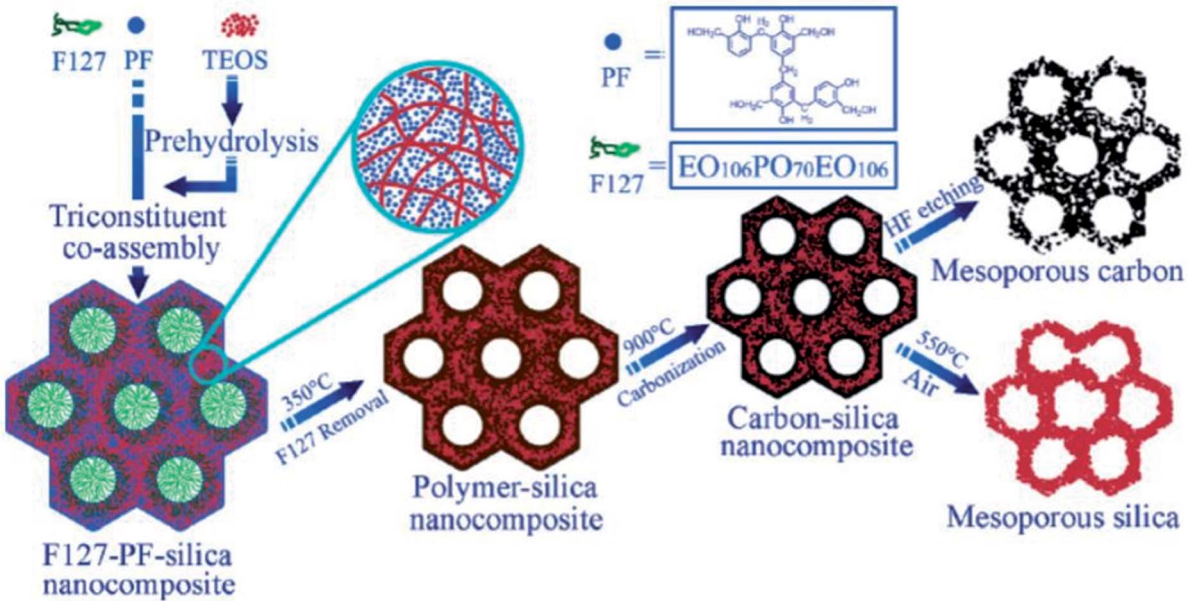

Fig. 18 A schematic illustration indicating a synthesis method for the fabrication of mesostructured polymer-silica nanocomposites.[103] Reprinted with permission from ref. 103. Copyright 2006 American Chemical Society.

The introduction of co-assembly/co-condensation approaches is not only applicable to oxidic systems but also to obtaining mesostructured channels of mixed semiconducting materials. These classes of mesostructured semiconductor materials have large specific surface areas of several hundreds of $m^2\ g^{-1}$, and the conductivity highly depends on the framework species. The combination of these characteristics makes these materials applicable to photonic, electronic and sensor applications.

The co-assembly of organic functional components. The co-assembly of organic functional components is another approach for synthesizing organic–inorganic hybrid mesostructured materials in the presence of a suitable template. Fig. 18 shows a schematic diagram of the fabrication of mesostructured polymer-silica nanocomposites. This method provides an opportunity to tune the mechanical stability of the mesostructured framework. *Via* this method, the fused functional components that typically possess hydrophobic nature interact with hydrophobic species present in the block-copolymer template or surfactant. An advantage of the co-assembly method is the high number of interfacial interactions between the organic functional components and the inorganic framework, which results in strong photophysical and mechanical characteristics. The incorporation of porphyrin dye components into mesostructured silica in the presence of a block co-polymer template can be taken as an example. In this case, tetraphenylporphyrin (TPP) foreign components desire to interact with amphiphilic triblock co-polymer types in a transparent medium, thus efficiently dispersing in the mesostructured silica host channels.[103]

There are other non-covalent functional components, such as conjugated polymers and surfactant-passivated nanoparticles, that can be applied to mesostructured inorganic–organic sites *via* a co-assembly method. Mesostructured materials can be modified with conjugated polymers for optoelectronic and electronic applications. For instance, hydrophobic sections of block co-polymer silica were combined with hydrophobic conjugated polymer sources, such as poly-[2-methoxy-5-(2′-ethyl-hexyloxy)-1,4-phenylenevinylene], under non-aqueous conditions.[104–106] Through controlling the template and solvent components, it is possible to improve the interfacial contact between the conjugated polymer particles and mesostructured network through a co-assembly synthesis method. Similarly, mesostructured materials can be functionalized with surfactant-passivated nanoparticles. Fan H. *et al.*[107] synthesized well-ordered three-dimensional nanocrystalline mesoporous gold nanoparticles through co-assembling hydrophilic nanocrystalline micelles within a silica framework (see Fig. 19). In this case, water was used as an intermediate for the soluble nanocrystals. The dimensions of the cells were tuned *via* adjusting the sizes of the nanocrystals and/or the chain lengths of the surfactants. Using an excess amount of the cross-linking silica source, co-assembly took place, fabricating an inorganic matrix near the gold nanoparticles with a hydrophobic nature. Non-covalent functional components have high potential to co-assemble, since they are highly compatible with inorganic sources, solvents and template components. These materials have the potential to incorporate *via* co-assembly into mesostructured matrices and to interact with several self-assembling components in only one synthetic step.

Post-synthetic functionalization approaches

Occasionally, one-pot synthetic approaches are not suitable to functionalize mesostructured materials with the desired microscopic characteristics. Post-synthetic modification is an approach in which mesostructured materials can be initially synthesized and subsequently functionalized *via* ordered steps to attain the desired properties. Post-synthetic modification

allows for the incorporation of multiple organic or inorganic functional species into a mesostructured system, which is not possible with an *in situ* modification route. In the case of organic functional components, post-synthetic incorporation regularly takes place between components on the inner mesopore surfaces, while for inorganic functional components, post-synthesis modification can take place between components at charged surface positions.[91]

Moreover, functional components with high surface loading can be incorporated into mesostructured frameworks with insignificant effects on the overall ordering of the as-synthesized material. However, there are limitations regarding some functional components with larger sizes than the diameters of the mesopores. In this case, they may not enter into the mesopore channels and can only concentrate around external particles, fibers, and film or monolith surfaces.

Prior to post-synthetic modification, there are some necessary treatments which must be carried out in order to obtain efficient modification results. The used template must be removed either by solvent extraction or oxidation procedures.[14] Besides, it is common to eliminate concentrations of hydroxyl groups from the surfaces of as-synthesized materials *via* mild/

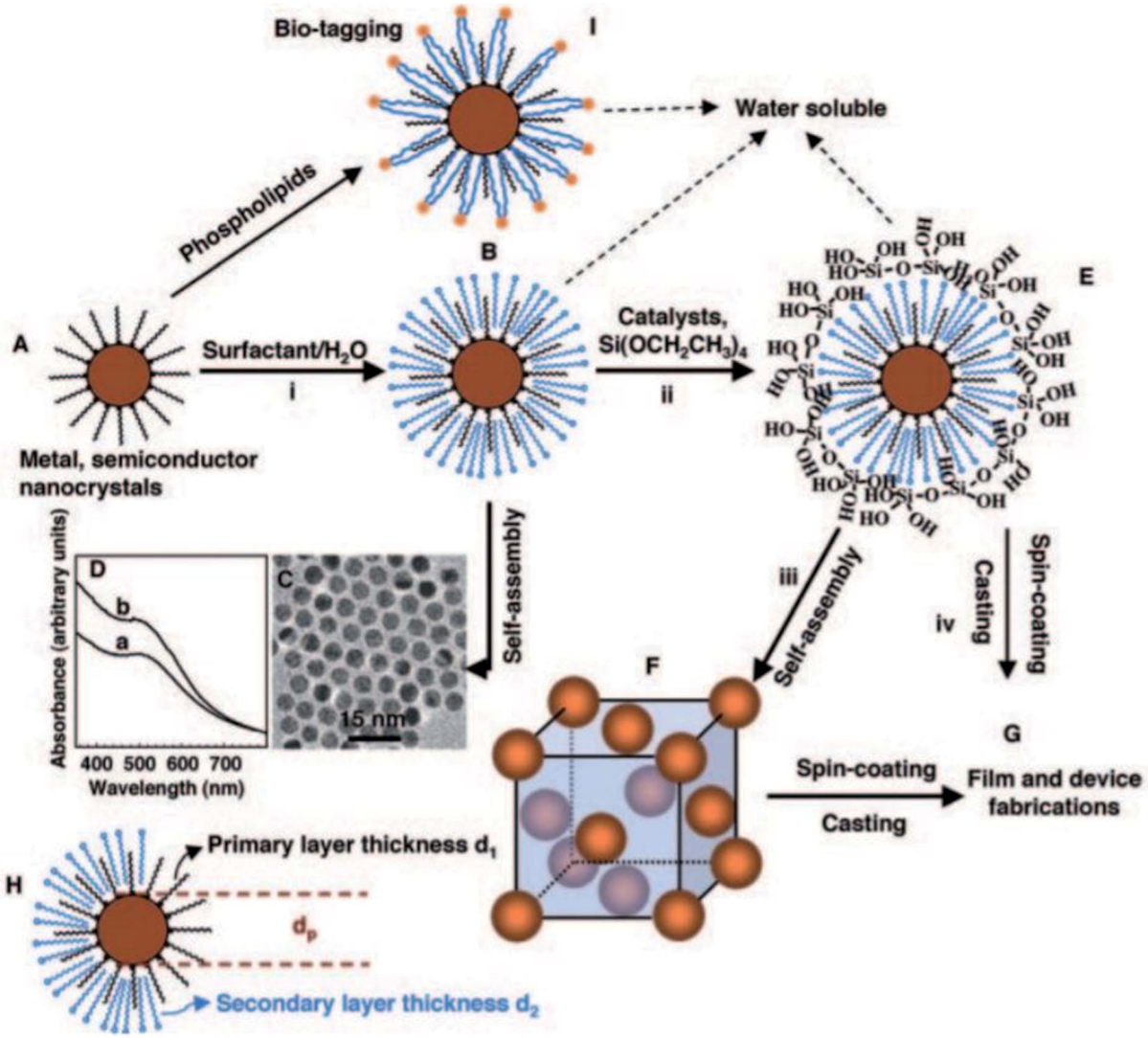

Fig. 19 A schematic illustration showing a synthesis method for the fabrication of water-soluble gold nanocrystal micelles and periodically ordered gold nanocrystal/silica mesostructures. (A) Gold nanocrystals were synthesized using 1-dodecanethiol as a stabilizing agent, where heat treatment was applied to additionally narrow the size of the particles. (B) Thiol-stabilized nanocrystals were encapsulated into surfactants *via* an oil-in-water microemulsion technique to form water-soluble nanocrystal (NC) micelle structures that, after evaporation, (C) self-assemble to form hexagonally ordered NC arrays. (D) The UV-visible spectra of (a) gold nanocrystals in chloroform and (b) gold NC micelles in water. (E) Silicic acid moieties produced through the hydrolysis of TEOS were ordered at the hydrophilic surfactant–water interface of NC micelles, leading to a gold NC/silica mesophase (F) composed of NCs ordered in a periodic face-centered cubic lattice inside a strong silica framework. (G) Under acidic conditions, casting or spin-coating resulted in ordered thin-film NC/silica mesophases. (H) The lattice constant of the NC/silica mesophase was restricted by the nanocrystal size, the primary layer thickness of the alkanethiol, and/or the secondary layer thickness of the surfactant. (I) Lipids or polyethylene glycol surfactants were proposed to prepare biocompatible water-soluble NC micelles for bio-labeling.[107] Reprinted with permission from ref. 107. Copyright 2004 The American Association for the Advancement of Science.

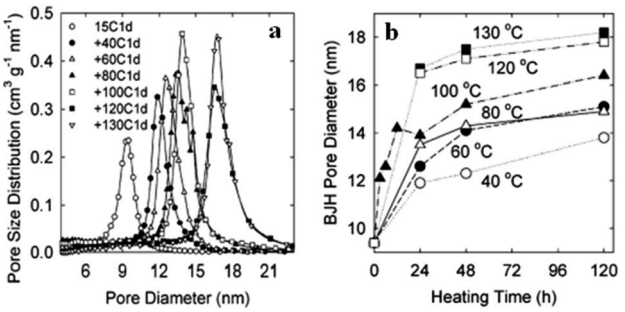

Fig. 20 Barrett, Joyner, and Halenda (BJH) pore size distributions for fabricated mesoporous SBA-15 samples hydrothermally treated (a) at various temperatures (40 °C to 130 °C) for 24 h and (b) for different periods of time (0–120 h) at various temperatures (40 °C to 130 °C).[110] Reprinted with permission from ref. 110. Copyright 2007 American Chemical Society.

high-temperature thermal treatments. According to recent research, post-heat treatment along with adjusting the pH value can significantly enhance the hydrothermal stability and textural properties, such as enlarging the pore size, increasing the surface area, and allowing uniform distributions.[108] Post-heat treatment (<100 °C) in water results in the blockage of mesopore channels.[109] Michal Kruk and Liang Cao[110] synthesized SBA-15 silica using the [$EO_{20}PO_{70}EO_{20}$] block co-polymer Pluronic P123 as a template in the presence of hexane as a hydrophobic swelling agent. They examined the effects of post-thermal treatment (40–130 °C) and different periods of treatment time. As shown in Fig. 20(a and b), obvious changes in the pore diameter were observed due to changing the operating temperature and length of thermal treatment. *Via* increasing the post-heating treatment temperature (up to 130 °C) and period of time (up to 2 h), pore diameters were enlarged to larger values of around 16 nm and 18 nm, respectively.

Mesoporous materials are typically functionalized to retain certain characteristics for desired applications. Recently, great efforts have been focused on the post-functionalization of mesoporous mixed metal oxides or calcined silica to covalently incorporate a large diversity of organic or inorganic components for catalysis, absorber and separation applications. In research done by our group, post-sulfonation treatment was applied to functionalize as-prepared mesoporous ZnO material with sulfonic groups (–SO_3H), used for the esterification of FFA to produce biodiesel.[111] The strategy for the post-sulfonation of the as-synthesized C@Zn core–shell solid is displayed in Fig. 21. During the sulfonation process, zinc oxide and SO_3H functional groups interact electrostatically together through hydrogen bonding groups to enrich the mesopore channels. The pore size decreased significantly from 3.45 nm to 3.16 nm after post-acid treatment, proving that functional components were positioned in the internal pores of the surface. Moreover, the

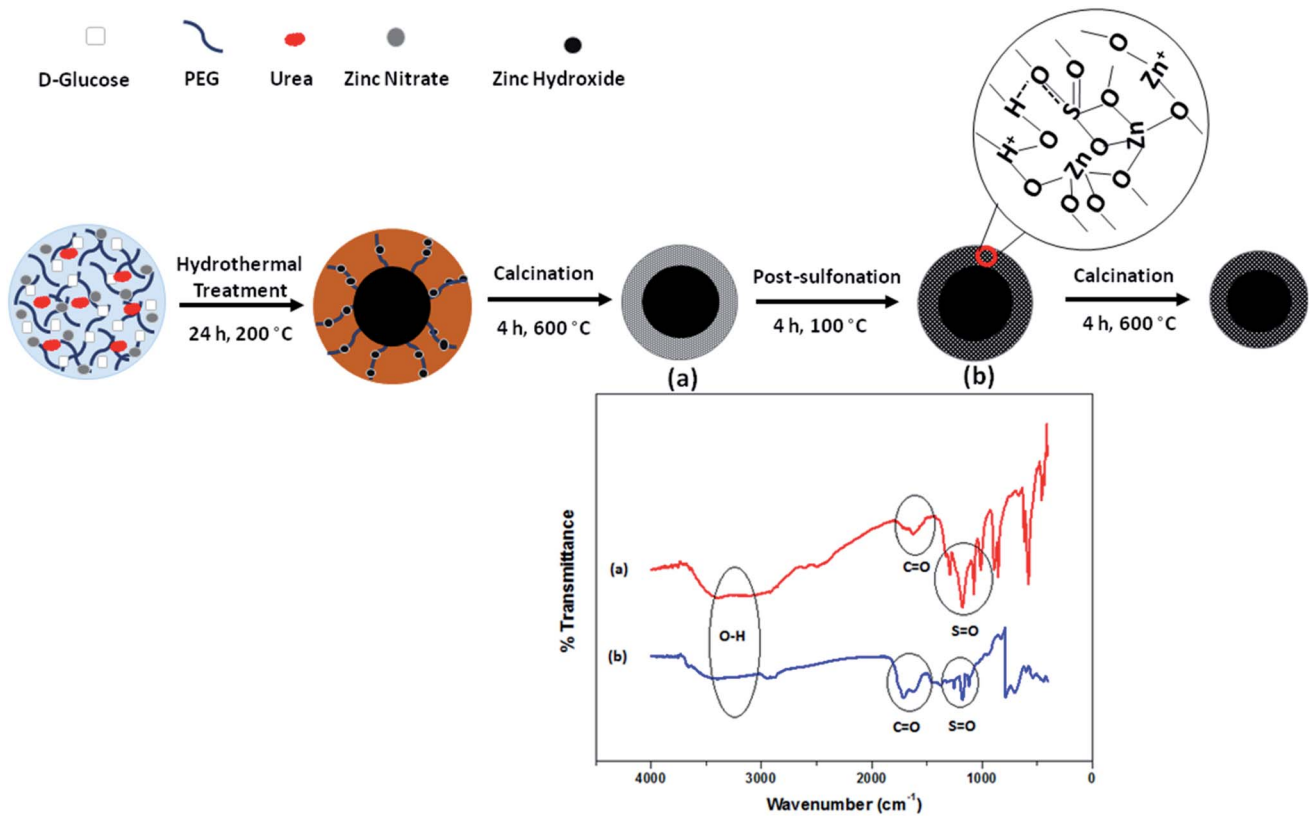

Fig. 21 A schematic representation of the post-sulfonation of as-prepared mesoporous ZnO material to fabricate a hydrophobic heterogeneous catalyst used for ester production. FTIR spectra of mesoporous ZnO (a) and SO_3H–ZnO (b) are provided for a comparative study.[111] Reprinted with permission from ref. 111. Copyright 2017 Elsevier.

Table 3 The effects of various sulfonation temperatures on the textural properties of a polymeric mesoporous mixed metal oxide ($ZnAl_2O_4$) material.[90] Reprinted with permission from ref. 90. Copyright 2016 Elsevier

Catalyst	S_{BET}[a]	D_p[b]	V_p[c]	Acid density[d]
Fresh $ZnAl_2O_4$	396.58	3.45	0.14	0.19 ± 0.05
SO_3H-$ZnAl_2O_4$ (100 °C)	399.66	3.21	0.15	1.39 ± 0.05
SO_3H-$ZnAl_2O_4$ (120 °C)	352.39	3.10	0.13	1.95 ± 0.07
SO_3H-$ZnAl_2O_4$ (140 °C)	301.65	2.73	0.10	2.28 ± 0.10
SO_3H-$ZnAl_2O_4$ (200 °C)	189.81	2.11	0.04	4.17 ± 0.07

[a] Specific surface area ($m^2\ g^{-1}$). [b] Average pore diameter (nm). [c] Total pore volume at P/P_o = 0.99 ($cm^3\ g^{-1}$). [d] Based on ammonia temperature programmed desorption (NH_3-TPD) measurements (mmol g^{-1}).

hydrophobicity of the functionalized catalyst was confirmed based on the absence of hydroxyl groups in the FTIR spectra in comparison with the unfunctionalized material.

In another research work, we hydrothermally synthesized polymeric mesoporous mixed metal oxide ($ZnAl_2O_4$) materials and then functionalized them with benzene-sulfonic acid under reflux conditions and a flow of N_2.[90] Furthermore, the effects of different sulfonation temperatures on the textural characteristics of the parent material were examined, as indicated in Table 3. The post-sulfonation temperature had a significant effect on the textural properties, and the surface area (399.66–189.81 $m^2\ g^{-1}$) and porosity (3.21–2.11 nm) were reduced at high temperatures. It is worth mentioning, however, that although the pore size sharply dropped upon raising the sulfonation temperature to 200 °C, the mesostructured framework was preserved. This might be attributed to the successfully attachment of sulfonic compounds to the inner pores of the surface.

Fig. 22 shows a schematic illustration of the polymeric and nonpolymeric post-sulfonation treatment of an as-synthesized mesoporous $ZnAl_2O_4$ material. It reveals that post-sulfonation treatment using a polymeric approach provided more opportunities to attach acid functional groups to the surfaces of active sites. It should be noted that the diffusion of polar by-products to the surface of the catalyst causes the deactivation of the catalyst.[112] Moreover, the synthesized mesoporous SO_3H–$ZnAl_2O_4$ catalyst was simply recovered and recycled, which significantly reduced the cost of production.[113] As a consequence, reusable eco-friendly solid acid catalysts have the potential to replace environmentally unfriendly homogeneous acid catalysts.[114] The synthesized mesoporous SO_3H–$ZnAl_2O_4$ catalyst was further utilized for methyl ester production, where the synthesized catalyst was able to stay highly active for eight continuous esterification reaction cycles without needing further recovery.[115] The CHNS results revealed that the sulfur content leaching was insignificant from the first to the eighth cycle (dropped from 2.23 to 1.50 wt%). The remarkable stability of the synthesized mesoporous SO_3H–$ZnAl_2O_4$ catalyst corresponded to the polymeric attachment of SO_3H groups to the inner pore walls under proper post-sulfonation conditions.[116] The same strategy was recently used to synthesize core–shell ZnO–TiO_2 hollow spheres[117] and a mesoporous NiO–ICG core–shell solid sphere catalyst[118] *via* an *in situ* hydrothermally assisted method for ester production applications.

The post-synthesis acid functionalization of mesoporous silica materials for catalysis applications can be carried out to maximize the activities and selectivities of these mesoporous materials *via* strengthening the acidity and, ultimately, the hydrophobicity. As an example, organosulfonic mesoporous silicas were synthesized and further post-functionalized with hydrophobic organic species.[119] The post-synthesis acid functionalization affected the textural properties; the average pore size and total pore volume sharply declined, while the interior and exterior surface areas were highly improved. The decrease in porosity corresponded to the agglomeration of SO_3H functional groups in the pore channels. Also, the thermal stability of the functionalized mesoporous catalyst increased, as no further mass loss was found after 350 °C from the thermal gravimetric analysis (TGA) plot. The catalytic performance of the synthesized catalyst was finally evaluated for the esterification of FFA, resulting in a high conversion rate of 94% at 120 °C over 120 min. In another research work,[120] SO_3H-OMC was fabricated *via* the covalent post-attachment of –SO_3H-holding aryl radicals to the surface of a mesostructured material (see Fig. 23). Initially, three forms of mesoporous SBA-15 material were fabricated at three different operating temperatures (100 °C, 130 °C, and 150 °C), followed by post-sulfonation treatment in the presence of 4-benzene-diazoniumsulfonate and H_3PO_2 aqueous solution to modify OMC-100, OMC-130, and OMC-150 to OMC-SO_3H-100, OMC-SO_3H-130, and OMC-SO_3H-150,

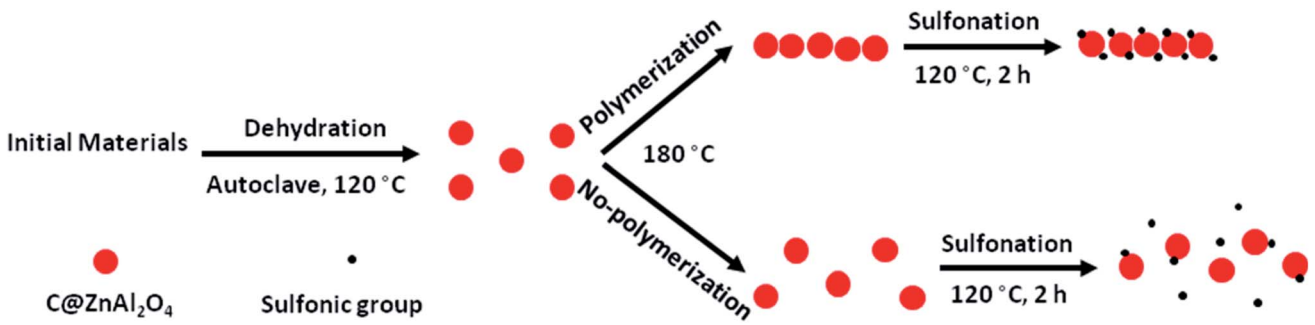

Fig. 22 A schematic illustration of the polymeric and non-polymeric post-sulfonation treatment of as-synthesized mesoporous carbon@$ZnAl_2O_4$ material.[115] Reprinted with permission from ref. 115. Copyright 2016 Elsevier.

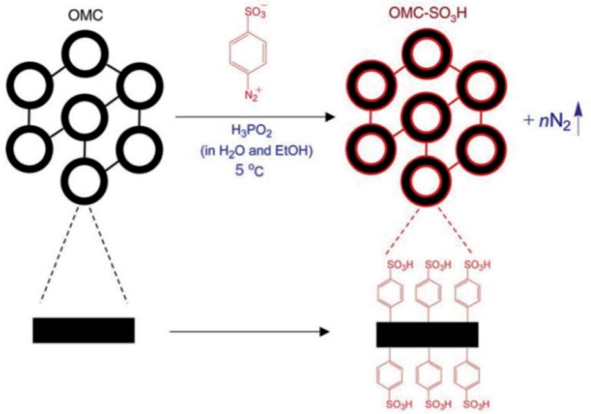

Fig. 23 A schematic representation of the post-synthetic functionalization of mesoporous OMC with sulfonic acid reagents.[120] Reprinted with permission from ref. 120. Copyright 2008 Elsevier.

respectively. The effects of the temperature-dependent post-sulfonation treatment on the textural properties and catalytic performance were studied, and the results are summarized in Table 4.[120]

Yasutaka Kuwahara *et al.*[121] functionalized mesoporous zirconosilicate with sulfonic functional groups using direct and post-synthesis sulfonation in the presence of ammonium sulfate ($(NH_4)_2SO_4$). According to the obtained results, direct-sulfonation gave a higher surface area than the other method, while samples synthesized *via* post-synthesis acid treatment possessed larger pore diameters and higher acid densities. This proves that the formation of larger pore diameters provides better opportunities for sulfonic functional species to successfully be incorporated into mesopore channels. Both prepared catalysts were applied to the esterification of FFA, and higher FFA conversion was achieved over the post-sulfonated mesoporous zirconosilicate catalyst in comparison with the one-pot functionalized mesoporous zirconosilicate catalyst.

Recently, considerable efforts have been devoted to employing functionalized mesoporous inorganic materials as supports for enhancing heterogeneous counterparts of homogeneous catalysts due to their well-suited textural characteristics.[16] To date, a wide range of organometallic species, such as Mo, Mn, Ir, Rh, and Pd, have been incorporated into mesostructured inorganic supports.[122,123] These classes of heterogenous materials not only satisfy environmental concerns regarding recovery and recyclability, but also enhance catalytic performance compared to homogenous samples. It has been reported that mesoporous MCM-41 combined with Pd components resulted in higher hydrogenation selectivity and reactivity in comparison with its homogenous counterparts due to considerable interactions between the mesoporous support and active metal species. It is worth mentioning that the existence of uniform and large diameter mesopores gives the opportunity to large species to be incorporated post-synthetically into interior mesopore sites, which can significantly enhance the dynamics, stabilities and performances of materials obtained under various reaction conditions. Generally, the main challenge is to control the incorporation of guest species into as-synthesized mesostructured materials to avoid agglomeration and the subsequent blockage of mesopore channels, which results in a loss of catalytic performance.[15]

These materials regularly display superior structural, physicochemical and textural properties, acidities, and catalytic performances in comparison with materials synthesized *via* co-condensation synthetic methods.[124] Post-modification can also be performed through the deposition of consecutive layers of various metal oxides on mesostructured silica. Fig. 24(a and b) shows a schematic diagram of hydrolytic and non-hydrolytic surface sol–gel synthetic methods.[125]

Aluminosilica is a very common example of this type, where $AlCl_3$ or $Al(NO_3)_3$ reacts with silanol species to synthesize mesoporous aluminosilica materials.[126–130] In comparison with the one-pot co-condensation method, this approach provides for the better diffusion of reactants into active sites due to modified surface Lewis/Brønsted acid spots.[131]

As another example, Cheralathan *et al.*[132] accomplished post-functionalization alumina distribution on the pore walls of mesoporous silica in the presence of inorganic aluminum salts using H_2O/NH_3 vapour as a hydrolyzing mediator at high temperature *via* an autoclave-assisted technique followed by calcination. In this procedure, aluminum salts were initially added into the mesopore channels of SBA-15 through a continuous multi-step wet impregnation approach; then, internal hydrolyzation took place based on H_2O/NH_3 vapour inside the autoclave at high temperature under autogenous pressure, homogeneously depositing aluminium hydroxide on the walls of SBA-15, which was followed by post-calcination treatment (Fig. 25). In this case, higher loadings of alumina could be

Table 4 The textural characteristic of mesoporous OMC and post-sulfonated SO_3H-OMC catalysts and the catalytic performance of SO_3H-OMC catalysts.[120] Reprinted with permission from ref. 120. Copyright 2008 Elsevier

Catalyst	S_{BET}[a]	Pore size[b]	Pore volume[c]	Acid density[d]	Conversion[e] (%)
OMC-100	1384	3.4	1.20	—	—
OMC-130	1338	4.5	1.52	—	—
OMC-150	1254	5.5	1.75	—	—
OMC-100-SO_3H	689	2.1	0.45	1.95	69.12
OMC-130-SO_3H	813	3.2	0.69	1.82	69.21
OMC-150-SO_3H	741	4.2	0.85	1.70	73.59

[a] Specific surface area ($m^2\ g^{-1}$). [b] Average pore diameter (nm). [c] Total pore volume at $P/P_o = 0.99$ ($cm^3\ g^{-1}$). [d] Determined *via* a titration method. [e] Esterification reaction conditions: catalyst concentration, 50 mg; ethanol, 0.05 mol; oleic acid, 0.005 mol; at 80 °C for 10 h.

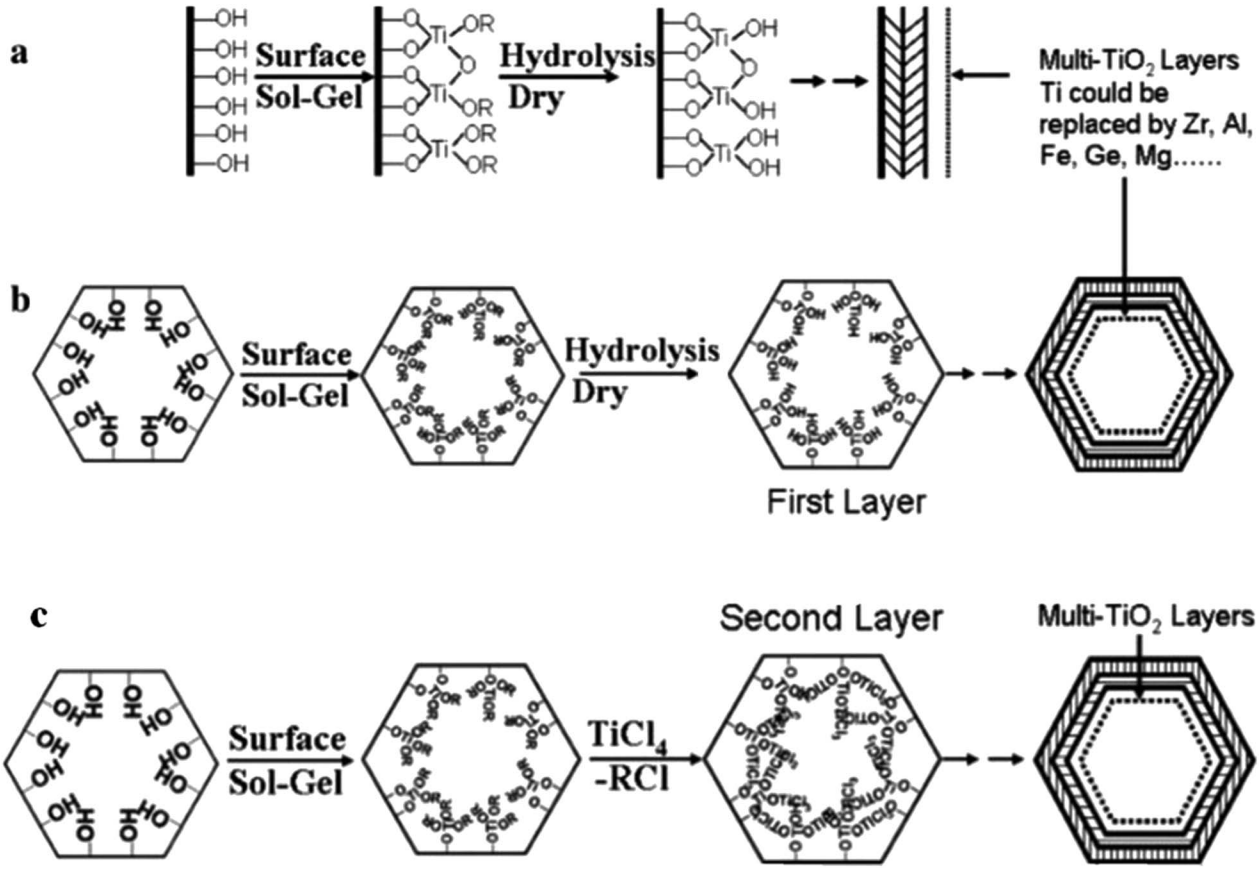

Fig. 24 A schematic diagram showing (a and b) hydrolytic and (c) non-hydrolytic surface sol–gel synthetic methods.[125] Reprinted with permission from ref. 125. Copyright 2005 American Chemical Society.

incorporated on the mesopore walls of SBA-15 with insignificant pore blocking and less crystallinity.

Along with transition/common metal oxides, rare-earth elements, such as Yb^{3+}, Er^{3+}, and Eu^{3+}, have been repeatedly applied as functional groups that electrostatically interact with the non-cationic surface areas of mesopore frameworks.[133,134]

An important point that needs to be taken into consideration is that there is a higher risk of the leaching or poisoning of supported species incorporated in the mesopore channels *via* post-functionalizing strategies compared to those prepared *via in situ* approaches. In fact, supported components are generally positioned on internal mesopore surfaces where they interact with other dispersing and reacting components in the mesopore framework.

Hybrid mesoporous compounds, particularly immobilized mesoporous silica nanoparticles, involve the strong binding of organic ligands and their corresponding metal complexes to inorganic matrices. The immobilization of metal complexes can significantly enhance the surface characteristics of these mesoporous materials to maximize their interactions with biological targets.[135] Eduardo Guimarães Vieira *et al.* immobilized two oxindolimine complexes based on zinc(II) and copper(II) which can act as carriers of water-insoluble anticancer metallodrugs.[136] The immobilization of the studied complexes on the MCM-41 matrices was done as follows. Initially, solutions of the oxindolimine-copper(II) complex and the analogous zinc(II) complex were prepared at a pH value of ~6.4. Modified and unmodified MCM-41 was added to each complex solution, and the mixtures were kept under constant stirring for 24 h at room temperature. Next, materials were filtrated and washed a number of times with a mixture of H_2O/dimethyl sulfoxide

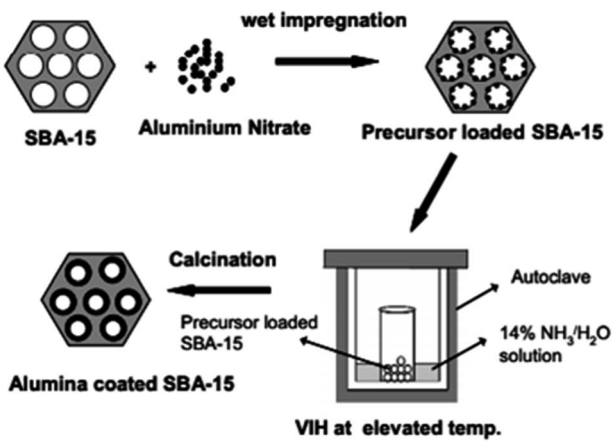

Fig. 25 A schematic diagram of post-functionalization alumina distribution on the pore walls of mesoporous silica *via* the VIH method.[132] Reprinted with permission from ref. 132. Copyright Elsevier.

Table 5 Structural parameters for the immobilization of complexes on the matrices.[136] Reprinted with permission from ref. 136. Copyright 2019 RSC

Sample	BET surface area ($m^2\ g^{-1}$)	Pore volume ($cm^3\ g^{-1}$)
MCM-41	1018	1.225
MCM-[Cu(isapn)]	525	0.269
MCM-[Zn(isapn)]	641	0.461
MCM-atzac	716	0.365
MCM-atzac-[Cu(isapn)]	365	0.333
MCM-atzac-[Zn(isapn)]	801	0.382

and then dried at 70 °C overnight. The BET results confirmed the presence of a type IV nitrogen adsorption isotherm and H1 hysteresis loop, indicating a class of hexagonal cylinder MCM-41 (Table 5). After the immobilization of the copper(II) or zinc(II) complexes on the modified and unmodified MCM-41 matrices, the surface areas and pore volumes decreased significantly. The exception was MCM-atzac-Zn, as both its surface area and pore volume showed higher values in comparison with the MCM-atzac precursor. In fact, stronger interactions between the MCM-atzac matrix and the zinc complex 2 through an immobilization process caused the occupation of the internal pore channels and an external expansion of its distribution, resulting in an enhancement of the surface area and pore volume.

The XRD diffractograms of MCM-atzac confirm the disappearance of the (110) and (200) reflections and the shifting of the (100) reflection toward higher angles in comparison with the other materials. This could be attributed to the attachment of atzac functional groups to the matrix (see Fig. 26).

Mesoporous silica nanoparticles have been similarly developed as nanocarriers for metal-based complexes. Mesoporous silica nanoparticles also possess remarkable characteristics as nanocarriers, including chemical stability, tunable pore size, and the ability for simple surface adaptation in the presence of various functional species for subsequent drug conjugation. In a series of experiments, mesoporous silica nanoparticles were employed as carriers for tin, titanium, and ruthenium complexes.[137–139] It was reported that the entire nanostructure of the mesoporous silica–drug conjugate was associated with setting off cancer cell apoptosis, and merely a minor release of the encapsulated metallodrug created cytotoxic effects. This study was innovative, as it pointed in the direction of a non-classical strategy of action compared to those regularly perceived for these sorts of systems. Besides, it was found that the existence of the nanostructure and the minor release of metallodrug from mesoporous silica nanoparticles were the causes associated with the death of cancer cells.

For controlled release applications like drug delivery, functionalized mesostructured inorganic materials can be applied to adjust mass transfer *via* changing the rate of desorption of an adsorbed compound.[140] In this case, the organic surface functionalization of mesostructured silica is an approach for controlling drug release *via* modifying the surface-binding

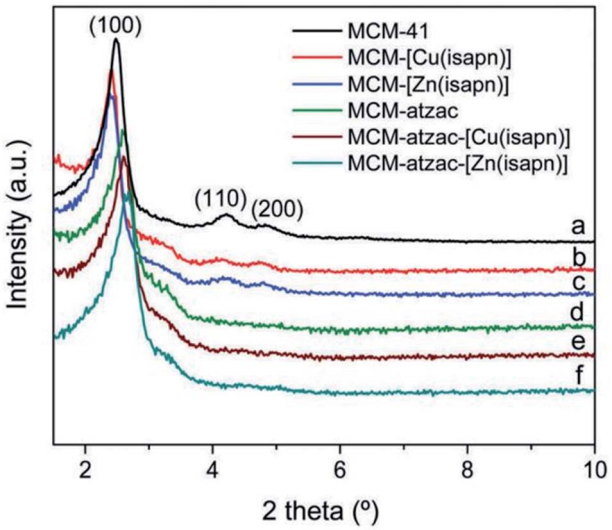

Fig. 26 XRD diffractograms of copper(II) and zinc(II) complexes immobilized on modified and unmodified matrices.[136] Reprinted with permission from ref. 136. Copyright 2019 RSC.

characteristics. As an example, the release rate of ibuprofen from mesoporous silica could be significantly improved upon introducing various organic functional species to the exteriors of internal mesopores. In fact, the incorporation of organic species enhances the hydrophilic nature of the mesopore surfaces, therefore affecting ibuprofen binding strength and subsequently enhancing the desorption degree. The novel post-functionalization of mesoporous SBA-15 was proposed by Blanca González,[141] where three generations (named G1, G2, and G3) of poly(propyleneimine) dendrimers with 4, 8 and 16 primary amine functional groups, respectively, at their periphery were covalently incorporated into a mesoporous framework *via* post-synthesis grafting (see Fig. 27(a)). The performance of these novel materials as controlled delivery devices was examined through studying the adsorption and release rates of ibuprofen (see Fig. 27(b)). The total ibuprofen loaded into these post-functionalized mesoporous SBA-15 materials gradually increased from 21.5% in pure SBA-15 to 28.8%, 40.8% and 48.0% in SBA-15-G1, SBA-15-G2, and SBA-15-G3, respectively. Ibuprofen release was fitted using the Higuchi model: $[IBU] = kt^{1/2}$, where IUB represents the amount of ibuprofen released against time t, and k represents a kinetic constant. According to the proposed model, there is a linear association between the square root of time and the ibuprofen released; by gradually increasing the dendrimer generation from G1 to G3, ibuprofen release increased, confirming the excellent drug release conditions. Therefore, the adsorption and release rates of a drug can be effectively controlled *via* the selection of a proper dendrimer group for modifying mesoporous silica. In a comparative study, amine functionalized mesoporous silica gave slower rates of ibuprofen release, which was consistent with the less hydrophilic nature of its surface.[142]

Amorphous silica materials have the potential to be applied to controlled release procedures due to their advantageous characteristics, including their isolated, uniform and large

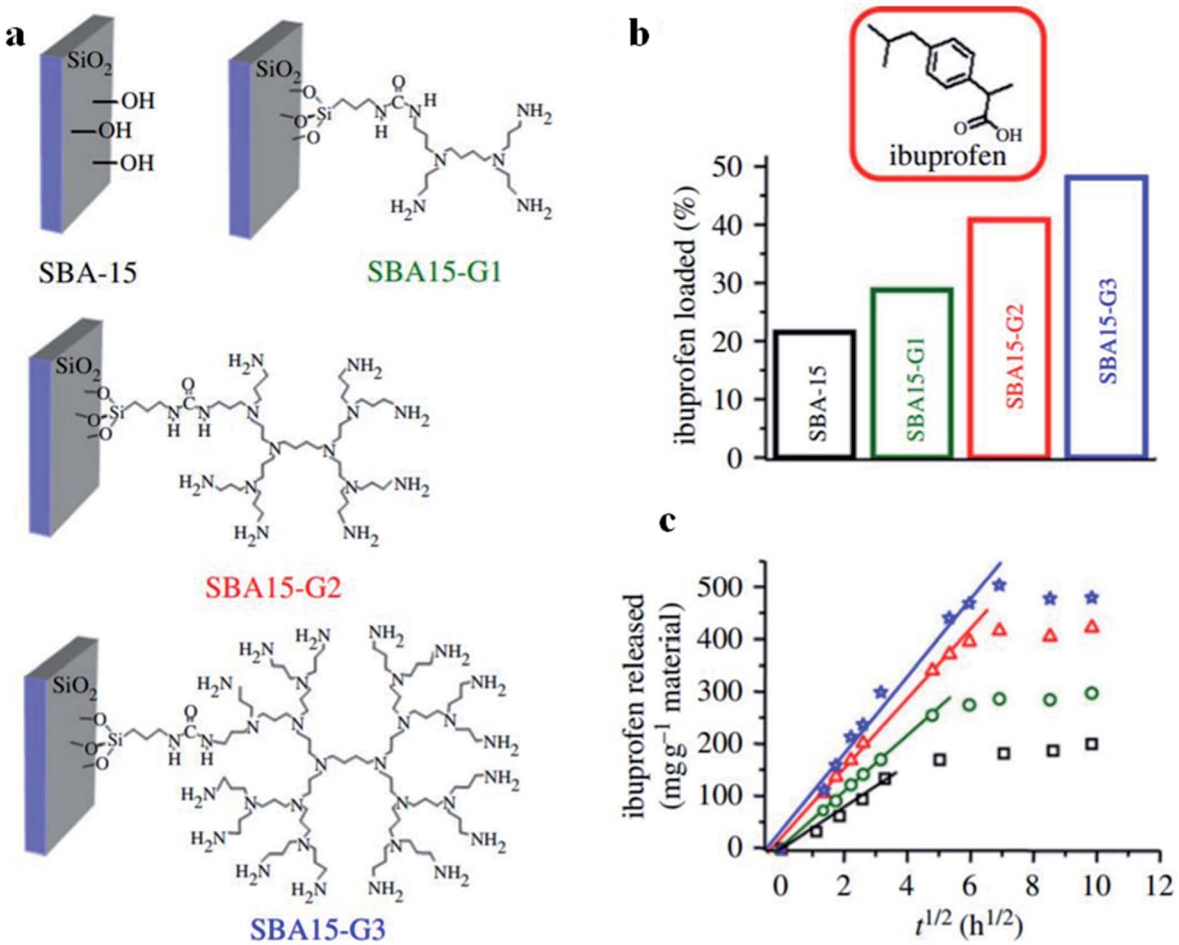

Fig. 27 (a) A schematic representation of pure SBA-15 and post-functionalized SBA-15-G1, SBA-15-G2, and SBA-15-G3, using poly(-propyleneimine) dendrimers. (b) Ibuprofen loading percentages and (c) ibuprofen released against time by pure SBA-15 and post-functionalized SBA-15-G1, SBA-15-G2, and SBA-15-G3; squares: pure SBA-15; stars: SBA15-G1; circles: SBA15-G2; triangles: SBA15-G3;[141] modified from ref. 140. Reprinted with permission from ref. 140 and 141. Copyright 2009 and 2012 respectively RSC.

diameter pore voids, which can host guest components. In this case, each isolated pore void could be a nanoscale host for foreign molecules. An alternate technique to control release rates is to control the mass transfer of guest molecules from the components that act as molecular gates to the interior/exterior of the mesostructured matrix.[143] An intermolecular reversible photodimerization–cleavage cycle is reported as a promising post-synthetic modification approach to regulate access to mesopore channels. Irradiation from 250 nm UV light causes the cleavage of the coumarin dimer, regenerating its monomer. Subsequently, the "double doors" of mesoporous silica will be broken, resulting in the release of foreign components. However, irradiation from UV light with a wavelength higher than 310 nm is insufficient to open the "double doors" of the mesopore channels, resulting in the trapping of guest particles inside the pores. The "open/closed double doors" methodology is highly promising for the photo-switchable controlled release of various species.[144] The modified pore voids are expected to provide more effective control of the passage of guest molecules through molecular gates than unmodified ones.

Through a post-synthesis oxidation approach, introduced thiol groups can be oxidized *via* a post-synthetic method. However, the main drawback to this post-synthesis oxidation method is that the good preservation of the mesopore structure cannot be guaranteed. Through *in situ* oxidation, the oxidation of thiol functional groups is concurrent with the formation of the mesostructured material. This is the best approach to counter the collapse of the mesopore walls due to the post-synthesis oxidation approach.[145–149] Mesoporous catalysts synthesized *via in situ* oxidation possess remarkable characteristics, such as high surface areas, uniform and large pores, and good mechanical and thermal stabilities, making them favourable for various catalytic applications.[150–156]

Summary and outlook

The main key to the wide-ranging potential applications of mesoporous inorganic materials is the ability for their interior pore channels and surface areas to be modified using numerous organic/inorganic components. Up to now, numerous synthetic schemes have been proposed to attain better control through

the incorporation and distribution of functional components within the mesostructured matrix. Through the cautious selection of components and reaction conditions, functional species could be selectively diffused on the internal surfaces of mesopore channels or within the mesopore wall frameworks. The availability of a large number of functionalization options presents an increased opportunity to design and synthesize these materials, continuing with the suitable modification of the structural, textural, and physicochemical properties of these materials, particularly at the molecular level. The use of both organic and inorganic functional components, such as common or transition metal oxides, rare-earth elements, and acid/base agents, to functionalize mesoporous inorganic materials has been increasingly exercised through either *in situ* (co-assembly/co-condensation) or post-synthetic functionalization strategies based on a variety of physicochemical interactions.

Generally, broadening the range of characteristics of mesoporous materials to expand their range of possible applications greatly requires expanding and diversifying the composition of mesoporous materials. It is essential to adjust the interfacial characteristics *via* surface functionalization procedures in order to develop their functionalities. Moreover, the hierarchical frameworks and porosities, in particular pore geometry, pore size, pore volume, and wall thickness, which are related to the performances of mesoporous materials, should be well established, and interfacial shortcomings require additional research. On the other hand, studies should also focus on multi-component and multi-layered mesopore structures, obtained *via* multiple templates, which could lead to unpredicted effects that are likely to allow multi-functional materials to be exploited for various applications. To sum up, the preparation and functionalization of mesoporous materials should move in the following corresponding directions: (i) the development of nanotechnology should cover more varieties of precursors for templated mesostructures; (ii) comparative analyses of the interactions between templating components and precursors under various synthesis conditions should be carried out; and (iii) the exploration of expendable and eco-friendly templates for synthesizing mesoporous materials with more industrial value should be conducted. Although some topics have already been well developed, much remains to be explored and discovered.

Abbreviation

NH_3-TPD	Ammonia temperature programmed desorption
ERS-8	Amorphous microporous silica-alumina
BJH	Barrett, Joyner and Halenda
BET	Brunauer–Emmett–Teller
DLCT	Direct liquid crystal templating
DBSA	Dodecylbenzenesulfonic acid
EISA	Evaporation induced self-assembly
FTIR	Fourier-transform infrared spectroscopy
FFA	Free fatty acid
M41S	Group name of mesoporous MCM materials
HMS	Hexagonal mesoporous silica
HRTEM	High resolution transmission electron microscopy
MSA	Mesoporous silica alumina
MCF	Mesostructured cellular foam
MSN	Mesostructured silica nanoparticle
MSU	Michigan State University
MCM	Mobil Composition of Matter
MDD	Molecular designed dispersion
NC	Nanocrystal
OMS	Ordered mesoporous silica
PMO	Periodic mesoporous organosilica
PHTS	Plugged hexagonal templated silica
PEG	Polyethylene glycol
PEO	Polyethylene oxide
PPO	Polypropylene oxide
SBA	Santa Barbara Amorphous
SEM	Scanning electron microscopy
S_{BET}	Specific surface area based on BET
TMO	Templated mesostructured transition metal oxide
TEOS	Tetraethylorthosilicate
TPP	Tetraphenylporphyrin
TGA	Thermal gravimetric analysis
TEM	Transmission electron microscopy
XRD	X-ray diffraction

Conflicts of interest

There are no conflicts to declare.

Acknowledgements

The authors would like to extend their profound gratitude to the Universiti Putra Malaysia (UPM) for financial support that funded this research work through Geran Putra UPM GP-IPB/2016/9515200. We also would like to convey our deepest gratitude and appreciation to Dr Maryam Shad for her ceaseless support.

References

1 K. Szczodrowski, B. Prélot, S. Lantenois, J. Zajac, M. Lindheimer, D. Jones, A. Julbe and A. van der Lee, *Microporous Mesoporous Mater.*, 2008, **110**, 111–118.
2 E. B. Celer and M. Jaroniec, *J. Am. Chem. Soc.*, 2006, **128**, 14408–14414.
3 N. D. Petkovich and A. Stein, *Chem. Soc. Rev.*, 2013, **42**, 3721–3739.
4 N. Pal and A. Bhaumik, *Adv. Colloid Interface Sci.*, 2013, **189–190**, 21–41.
5 R. Hosseinzadeh, K. Khorsandi and S. Hemmaty, *PLoS One*, 2013, **8**, e57353.
6 T. Wagner, S. Haffer, C. Weinberger, D. Klaus and M. Tiemann, *Chem. Soc. Rev.*, 2013, **42**, 4036–4053.
7 W. Li and D. Zhao, *Chem. Commun.*, 2013, **49**, 943–946.
8 A. J. Schwanke, R. Balzer and S. Pergher, in *Micro and Nano Technologies*, ed. C. B. T.-H. of N. for I. A. Mustansar Hussain, Elsevier, 2018, pp. 908–915.

9 P. Hesemann, T. P. Nguyen and S. El Hankari, *Materials*, 2014, **7**, 2978–3001.
10 V. Meynen, P. Cool and E. F. Vansant, *Microporous Mesoporous Mater.*, 2009, **125**, 170–223.
11 S. Soltani, U. Rashid, S. I. Al-Resayes and I. A. Nehdi, *Energy Convers. Manag.*, 2017, **141**, 183–205.
12 T.-Y. Ma, L. Liu and Z.-Y. Yuan, *Chem. Soc. Rev.*, 2013, **42**, 3977–4003.
13 S. S. Park, M. Santha Moorthy and C.-S. Ha, *Npg Asia Mater*, 2014, **6**, e96.
14 C. Perego and R. Millini, *Chem. Soc. Rev.*, 2013, **42**, 3956–3976.
15 Q. Huo, *Synthetic Chemistry of the Inorganic Ordered Porous Materials*, Elsevier, Amsterdam, 2011, ch. 16, pp. 339–373.
16 W. Xin and Y. Song, *RSC Adv.*, 2015, **5**, 83239–83285.
17 C. T. Kresge and W. J. Roth, *Chem. Soc. Rev.*, 2013, **42**, 3663–3670.
18 Y. Wan and D. Zhao, *Chem. Rev.*, 2007, **107**, 2821–2860.
19 B. A. Holmberg, H. Wang and Y. Yan, *Microporous Mesoporous Mater.*, 2004, **74**, 189–198.
20 G. Crépeau, V. Montouillout, A. Vimont, L. Mariey, T. Cseri and F. Maugé, *J. Phys. Chem. B*, 2006, **110**, 15172–15185.
21 C. Perego, S. Amarilli, A. Carati, C. Flego, G. Pazzuconi, C. Rizzo and G. Bellussi, *Microporous Mesoporous Mater.*, 1999, **27**, 345–354.
22 L. Zhang, J. Yan, M. Zhou, Y. Yang and Y.-N. Liu, *Appl. Surf. Sci.*, 2013, **268**, 237–245.
23 L. Zhang, J. Yan, M. Zhou, Y. Yu, Y. Liu and Y. Liu, *Trans. Nonferrous Met. Soc. China*, 2014, **24**, 743–749.
24 S. K. Mehta and G. Kaur, *Microemulsions: Thermodynamic and Dynamic Properties*, 2011, pp. 381–406.
25 D. Lombardo, P. Calandra, D. Barreca, S. Magazù and M. A. Kiselev, *Nanomaterials*, 2016, **6**, 125–151.
26 J. Silvestre-Albero, A. Sepúlveda-Escribano and F. R. Reinoso, *Microporous Mesoporous Mater.*, 2008, **113**, 362–369.
27 A. C. Pradhan, A. Paul and G. R. Rao, *J. Chem. Sci.*, 2017, **129**, 381–395.
28 D. M. Bezerra, I. W. Zapelini, K. N. Franke, M. E. Ribeiro and D. Cardoso, *Mater. Charact.*, 2019, **154**, 103–115.
29 F. Carniato, C. Bisio, G. Paul, G. Gatti, L. Bertinetti, S. Coluccia and L. Marchese, *J. Mater. Chem.*, 2010, **20**, 5504–5509.
30 D. Rath, S. Rana and K. M. Parida, *RSC Adv.*, 2014, **4**, 57111–57124.
31 A. J. Schwanke, R. Balzer and S. Pergher, *Handbook of Ecomaterials*, ed. L. M. T. Martínez, O. V. Kharissova and B. I. Kharisov, Springer International Publishing, Cham, 2017, pp. 1–22.
32 C. Gérardin, J. Reboul, M. Bonne and B. Lebeau, *Chem. Soc. Rev.*, 2013, **42**, 4217–4255.
33 K. Wang, Y. Lin, M. A. Morris and J. D. Holmes, *J. Mater. Chem.*, 2006, **16**, 4051–4057.
34 C. R. P. Silva, F. da Rocha Ferreira, G. D. Webler, A. O. S. da Silva, F. C. de Abreu and E. J. S. Fonseca, *Mater. Res. Express*, 2017, **4**, 65402.
35 S. Iqbal and J. Il Yun, *RSC Adv.*, 2018, **8**, 32211–32220.
36 R. Narayan, U. Y. Nayak, A. M. Raichur and S. Garg, *Pharmaceutics*, 2018, **10**, 118.
37 V. Tkachenko, C. Matei Ghimbeu, C. Vaulot, L. Josien, L. Vidal, J. Poly and A. Chemtob, *Langmuir*, 2019, **35**, 16324–16334.
38 L. Gai, Z. Chen, H. Jiang, Y. Tian, Q. Wang and D. Cui, *J. Cryst. Growth*, 2006, **291**, 527–532.
39 D. Gao, A. Duan, X. Zhang, K. Chi, Z. Zhao, J. Li, Y. Qin, X. Wang and C. Xu, *J. Mater. Chem. A*, 2015, **3**, 16501–16512.
40 J. Herzberger, K. Niederer, H. Pohlit, J. Seiwert, M. Worm, F. R. Wurm and H. Frey, *Chem. Rev.*, 2016, **116**, 2170–2243.
41 R. M. Grudzien, B. E. Grabicka and M. Jaroniec, *Appl. Surf. Sci.*, 2007, **253**, 5660–5665.
42 P. F. Fulvio, B. E. Grabicka, R. M. Grudzien and M. Jaroniec, *Adsorpt. Sci. Technol.*, 2007, **25**, 439–449.
43 E. B. Celer, M. Kruk, Y. Zuzek and M. Jaroniec, *J. Mater. Chem.*, 2006, **16**, 2824–2833.
44 C.-L. Lin, Y.-S. Pang, M.-C. Chao, B.-C. Chen, H.-P. Lin, C.-Y. Tang and C.-Y. Lin, *J. Phys. Chem. Solids*, 2008, **69**, 415–419.
45 L. B. de O. Freitas, I. J. G. Bravo, W. A. de A. Macedo and E. M. B. de Sousa, *J. Sol-Gel Sci. Technol.*, 2016, **77**, 186–204.
46 B.-H. Min, E.-Y. Jeong, M. Thommes and S.-E. Park, *Chem. Commun.*, 2011, **47**, 4673–4675.
47 C. Herdes, M. A. Santos, S. Abelló, F. Medina and L. F. Vega, *Appl. Surf. Sci.*, 2005, **252**, 538–547.
48 P. Van Der Voort, P. I. Ravikovitch, K. P. De Jong, A. V Neimark, A. H. Janssen, M. Benjelloun, E. Van Bavel, P. Cool, B. M. Weckhuysen and E. F. Vansant, *Chem. Commun.*, 2002, **9**, 1010–1011.
49 S. Meoto, N. Kent, M. M. Nigra and M.-O. Coppens, *Microporous Mesoporous Mater.*, 2017, **249**, 61–66.
50 Y. Mao, Y. Zhou, H. Wen, J. Xie, W. Zhang and J. Wang, *New J. Chem.*, 2014, **38**, 3295–3301.
51 L. Hermida, J. Agustian, A. Z. Abdullah and A. R. Mohamed, *Open Chem.*, 2019, **17**, 1000–1016.
52 K. De Witte, V. Meynen, M. Mertens, O. I. Lebedev, G. Van Tendeloo, A. Sepúlveda-Escribano, F. Rodríguez-Reinoso, E. F. Vansant and P. Cool, *Appl. Catal., B*, 2008, **84**, 125–132.
53 J. Liu, C. Li, Q. Yang, J. Yang and C. Li, *Langmuir*, 2007, **23**, 7255–7262.
54 S.-Y. Chen and S. Cheng, *Chem. Mater.*, 2007, **19**, 3041–3051.
55 R. Gao, W.-L. Dai, X. Yang, H. Li and K. Fan, *Appl. Catal., A*, 2007, **332**, 138–145.
56 P. Schmidt-Winkel, W. Lukens Wayne, P. Yang, D. I. Margolese, J. S. Lettow, J. Y. Ying and G. D. Stucky, *Chem. Mater.*, 2000, **12**, 686–696.
57 X. Ma, H. Sun and P. Yu, *J. Mater. Sci.*, 2008, **43**, 887–891.
58 H. Zhong, G. Zhu, P. Wang, J. Liu, J. Yang and Q. Yang, *J. Chromatogr. A*, 2008, **1190**, 232–240.
59 J. Allouche, J.-C. Dupin and D. Gonbeau, *Chem. Commun.*, 2011, **47**, 7476–7478.
60 S. A. Bagshaw and I. J. Bruce, *Microporous Mesoporous Mater.*, 2008, **109**, 199–209.
61 Z. Jin, X. Wang and X. Cui, *J. Non-Cryst. Solids*, 2007, **353**, 2507–2514.

62 K. Biswas, J. C. Ray, J.-S. Choi and W.-S. Ahn, *J. Non-Cryst. Solids*, 2008, **354**, 1–9.
63 L. Zhang, L. Jin, B. Liu and J. He, *Front. Chem.*, 2019, **7**, 22.
64 M. A. A. Aziz, A. A. Jalil, S. Triwahyono, R. R. Mukti, Y. H. Taufiq-Yap and M. R. Sazegar, *Appl. Catal., B*, 2014, **147**, 359–368.
65 M. Davidson, Y. Ji, G. J. Leong, N. C. Kovach, B. G. Trewyn and R. M. Richards, *ACS Appl. Nano Mater.*, 2018, **1**, 4386–4400.
66 D. Xu, H. Lv and B. Liu, *Front. Chem.*, 2018, **6**, 550.
67 K. An and G. A. Somorjai, *Catal. Lett.*, 2015, **145**, 233–248.
68 M. Shamzhy, M. Opanasenko, P. Concepción and A. Martínez, *Chem. Soc. Rev.*, 2019, **48**, 1095–1149.
69 S. C. Warren, L. C. Messina, L. S. Slaughter, M. Kamperman, Q. Zhou, S. M. Gruner, F. J. DiSalvo and U. Wiesner, *Science*, 2008, **320**, 1748–1752.
70 N. Kosinov, C. Liu, E. J. M. Hensen and E. A. Pidko, *Chem. Mater.*, 2018, **30**, 3177–3198.
71 D. P. Sahoo, D. Rath, B. Nanda and K. M. Parida, *RSC Adv.*, 2015, **5**, 83707–83724.
72 Q. Tian, Z. Zhang, L. Yang and S. Hirano, *Electrochim. Acta*, 2014, **138**, 155–162.
73 J. Du, X. Lai, N. Yang, J. Zhai, D. Kisailus, F. Su, D. Wang and L. Jiang, *ACS Nano*, 2011, **5**, 590–596.
74 L. Chen, B. Yao, Y. Cao and K. Fan, *J. Phys. Chem. C*, 2007, **111**, 11849–11853.
75 M. A. Abdolahi Sadatlu and N. Mozaffari, *Sol. Energy*, 2016, **133**, 24–34.
76 L. Mahoney and R. T. Koodali, *Materials*, 2014, **7**, 2697–2746.
77 K. Na and G. A. Somorjai, *Catal. Lett.*, 2015, **145**, 193–213.
78 B. Niu, X. Wang, K. Wu, X. He and R. Zhang, *Materials*, 2018, **11**, 1910.
79 J. L. Vivero-Escoto, Y.-D. Chiang, K. Wu and Y. Yamauchi, *Sci. Technol. Adv. Mater.*, 2012, **13**, 13003.
80 J. H. Pan, X. S. Zhao and W. I. Lee, *Chem. Eng. J.*, 2011, **170**, 363–380.
81 S. Ribbens, V. Meynen, G. Van Tendeloo, X. Ke, M. Mertens, B. U. W. Maes, P. Cool and E. F. Vansant, *Microporous Mesoporous Mater.*, 2008, **114**, 401–409.
82 D. Fattakhova-Rohlfing, A. Zaleska and T. Bein, *Chem. Rev.*, 2014, **114**, 9487–9558.
83 C.-C. Tsai and H. Teng, *Chem. Mater.*, 2006, **18**, 367–373.
84 M. Shahrezaei, S. Habibzadeh, A. A. Babaluo, H. Hosseinkhani, M. Haghighi, A. Hasanzadeh and R. Tahmasebpour, *J. Exp. Nanosci.*, 2017, **12**, 45–61.
85 S. Sun, W. Wang, M. Shang, J. Ren and L. Zhang, *J. Mol. Catal. A: Chem.*, 2010, **320**, 72–78.
86 Z. Wu, Q. Li, D. Feng, P. A. Webley and D. Zhao, *J. Am. Chem. Soc.*, 2010, **132**, 12042–12050.
87 H. Ji, X. Liu, X. Wang and X. Yao, *J. Colloid Interface Sci.*, 2011, **353**, 356–362.
88 S. Soltani, U. Rashid, R. Yunus, Y. H. Taufiq-Yap and S. I. Al-Resayes, *Renewable Energy*, 2016, **99**, 1235–1243.
89 S. Soltani, U. Rashid, I. A. Nehdi and S. I. Al-Resayes, *Chem. Eng. Technol.*, 2017, **40**, 1931–1939.
90 S. Soltani, U. Rashid, R. Yunus and Y. H. Taufiq-Yap, *Fuel*, 2016, **178**, 253–262.
91 G. L. Athens, R. M. Shayib and B. F. Chmelka, *Curr. Opin. Colloid Interface Sci.*, 2009, **14**, 281–292.
92 S. Fujita and S. Inagaki, *Chem. Mater.*, 2008, **20**, 891–908.
93 N. Mizoshita, T. Tani and S. Inagaki, *Chem. Soc. Rev.*, 2011, **40**, 789–800.
94 Q. Yang, J. Liu, L. Zhang and C. Li, *J. Mater. Chem.*, 2009, **19**, 1945–1955.
95 S. Inagaki, S. Guan, T. Ohsuna and O. Terasaki, *Nature*, 2002, **416**, 304–307.
96 G. Morales, G. Athens, B. F. Chmelka, R. van Grieken and J. A. Melero, *J. Catal.*, 2008, **254**, 205–217.
97 Y. Chen, Y. Cao, Y. Suo, G.-P. Zheng, X.-X. Guan and X.-C. Zheng, *J. Taiwan Inst. Chem. Eng.*, 2015, **51**, 186–192.
98 L. Zhao, H. Qin, R. Wu and H. Zou, *J. Chromatogr. A*, 2012, **1228**, 193–204.
99 F. Mumtaz, M. Zuber, K. M. Zia, T. Jamil and R. Hussain, *Korean J. Chem. Eng.*, 2013, **30**, 2259–2263.
100 A. Drelinkiewicz, Z. Kalemba-Jaje, E. Lalik and R. Kosydar, *Fuel*, 2014, **116**, 760–771.
101 Q. Yang, J. Liu, J. Yang, M. P. Kapoor, S. Inagaki and C. Li, *J. Catal.*, 2004, **228**, 265–272.
102 Q. Yang, M. P. Kapoor, S. Inagaki, N. Shirokura, J. N. Kondo and K. Domen, *J. Mol. Catal. A: Chem.*, 2005, **230**, 85–89.
103 R. Liu, Y. Shi, Y. Wan, Y. Meng, F. Zhang, D. Gu, Z. Chen, B. Tu and D. Zhao, *J. Am. Chem. Soc.*, 2006, **128**, 11652–11662.
104 S. Neyshtadt, M. Kalina and G. L. Frey, *Adv. Mater.*, 2008, **20**, 2541–2546.
105 S. Kirmayer, E. Dovgolevsky, M. Kalina, E. Lakin, S. Cadars, J. D. Epping, A. Fernández-Arteaga, C. Rodríguez-Abreu, B. F. Chmelka and G. L. Frey, *Chem. Mater.*, 2008, **20**, 3745–3756.
106 E. Dovgolevsky, S. Kirmayer, E. Lakin, Y. Yang, C. J. Brinker and G. L. Frey, *J. Mater. Chem.*, 2008, **18**, 423–436.
107 H. Fan, K. Yang, D. M. Boye, T. Sigmon, K. J. Malloy, H. Xu, G. P. López and C. J. Brinker, *Science*, 2004, **304**, 567–571.
108 G. Wu, J. Li, Z. Fang, L. Lan, R. Wang, T. Lin, M. Gong and Y. Chen, *Chem. Eng. J.*, 2015, **271**, 1–13.
109 Z. Wu, P. A. Webley and D. Zhao, *J. Mater. Chem.*, 2012, **22**, 11379–11389.
110 M. Kruk and L. Cao, *Langmuir*, 2007, **23**, 7247–7254.
111 S. Soltani, U. Rashid, S. I. Al-Resayes and I. A. Nehdi, *J. Cleaner Prod.*, 2017, **144**, 482–491.
112 V. B. Veljkovic, S. H. Lakicevic, O. S. Stamenkovic, Z. B. Todorovic and M. L. Lazic, *Fuel*, 2006, 2671–2675.
113 F. Guo, Z. Fang, C. C. Xu and R. L. Smith, *Prog. Energy Combust. Sci.*, 2012, **38**, 672–690.
114 J. H. Clark and D. J. Macquarrie, *Chem. Commun.*, 1998, **8**, 853–860.
115 S. Soltani, U. Rashid, I. Arbi and S. I. Al-resayes, *J. Taiwan Inst. Chem. Eng.*, 2016, 1–10.
116 U. Rashid, S. Soltani, S. I. Al-Resayes and I. A. Nehdi, in *Metal Oxides*, Elsevier, 2018. pp. 303–319.
117 S. Soltani, N. Khanian, U. Rashid and T. S. Y. Choong, *Renewable Energy*, 2020, **151**, 1076–1081.

118 S. Soltani, N. Khanian, U. Rashid and T. S. Yaw Choong, *RSC Adv.*, 2019, **9**, 31306–31315.
119 I. Mbaraka and B. Shanks, *J. Catal.*, 2005, **229**, 365–373.
120 R. Liu, X. Wang, X. Zhao and P. Feng, *Carbon*, 2008, **46**, 1664–1669.
121 Y. Kuwahara, T. Fujitani and H. Yamashita, *Catal. Today*, 2014, **237**, 18–28.
122 P. Das, A. R. Silva, A. P. Carvalho, J. Pires and C. Freire, *J. Mater. Sci.*, 2009, **44**, 2865–2875.
123 Z. Huang, M. Brookhart, A. S. Goldman, S. Kundu, A. Ray, S. L. Scott and B. C. Vicente, *Adv. Synth. Catal.*, 2009, **351**, 188–206.
124 Y. Wang, K.-Y. Lee, S. Choi, J. Liu, L.-Q. Wang and C. H. F. Peden, *Green Chem.*, 2007, **9**, 540–544.
125 W. Yan, S. M. Mahurin, S. H. Overbury and S. Dai, *Chem. Mater.*, 2005, **17**, 1923–1925.
126 D. U. Tulyaganov, A. A. Reddy, V. V Kharton and J. M. F. Ferreira, *J. Power Sources*, 2013, **242**, 486–502.
127 M. R. Agliullin, V. P. Talzi, N. A. Filippova, V. R. Bikbaeva, S. V Bubennov, T. R. Prosochkina, N. G. Grigorieva, N. Narender and B. I. Kutepov, *Appl. Petrochem. Res.*, 2018, **8**, 141–151.
128 P. Sreenivasulu, N. Viswanadham and S. K. Saxena, *J. Mater. Chem. A*, 2014, **2**, 7354–7359.
129 N. Musselwhite, K. Na, K. Sabyrov, S. Alayoglu and G. A. Somorjai, *J. Am. Chem. Soc.*, 2015, **137**, 10231–10237.
130 J. Čejka and S. Mintova, *Catal. Rev.*, 2007, **49**, 457–509.
131 D. Srinivas and P. Ratnasamy, *Microporous Mesoporous Mater.*, 2007, **105**, 170–180.
132 K. K. Cheralathan, T. Hayashi and M. Ogura, *Microporous Mesoporous Mater.*, 2008, **116**, 406–415.
133 B. An, S. S. Park, Y. Jung, I. Kim and C.-S. Ha, *Mol. Cryst. Liq. Cryst.*, 2008, **492**, 210/[574]–220/[584].
134 E. Besson, A. Mehdi, C. Reyé and R. J. P. Corriu, *J. Mater. Chem.*, 2006, **16**, 246–248.
135 W. A. Wani, S. Prashar, S. Shreaz and S. Gómez-Ruiz, *Coord. Chem. Rev.*, 2016, **312**, 67–98.
136 E. Guimarães Vieira, R. B. Miguel, D. Rodrigues da Silva, R. Boni Fazzi, R. A. A. de Couto, J. H. Marin, M. L. A. Temperini, J. da Silva Shinohara, H. E. Toma, L. C. Russo, Y. T. Magalhães, N. L. Dias Filho, F. L. Forti and A. M. da Costa Ferreira, *New J. Chem.*, 2019, **43**, 386–398.
137 D. Díaz-García, D. Cenariu, Y. Pérez, P. Cruz, I. del Hierro, S. Prashar, E. Fischer-Fodor and S. Gómez-Ruiz, *Dalton Trans.*, 2018, **47**, 12284–12299.
138 Y. Ellahioui, M. Patra, C. Mari, R. Kaabi, J. Karges, G. Gasser and S. Gómez-Ruiz, *Dalton Trans.*, 2019, **48**, 5940–5951.
139 S. Gómez-Ruiz, A. García-Peñas, S. Prashar, A. Rodríguez-Diéguez and E. Fischer-Fodor, *Materials*, 2018, **11**, 224.
140 V.-R. María, I.-B. Isabel and C. Montserrat, *Philos. Trans. R. Soc., A*, 2012, **370**, 1400–1421.
141 B. González, M. Colilla, C. L. de Laorden and M. Vallet-Regí, *J. Mater. Chem.*, 2009, **19**, 9012–9024.
142 Q. Tang, Y. Xu, D. Wu, Y. Sun, J. Wang, J. Xu and F. Deng, *J. Controlled Release*, 2006, **114**, 41–46.
143 J. Kärger, T. Binder, C. Chmelik, F. Hibbe, H. Krautscheid, R. Krishna and J. Weitkamp, *Nat. Mater.*, 2014, **13**, 333–343.
144 C. L. Birmingham, V. Canadien, N. A. Kaniuk, B. E. Steinberg, D. E. Higgins and J. H. Brumell, *Nature*, 2008, **451**, 350.
145 D. Feng, T.-N. Gao, M. Fan, A. Li, K. Li, T. Wang, Q. Huo and Z.-A. Qiao, *NPG Asia Mater.*, 2018, **10**, 800–809.
146 X. Deng, K. Chen and H. Tüysüz, *Chem. Mater.*, 2017, **29**, 40–52.
147 E. Zhang, M. E. Casco, F. Xu, W.-B. Sheng, S. Oswald, L. Giebeler, K. Wegner, L. Borchardt and S. Kaskel, *Carbon*, 2019, **149**, 743–749.
148 J. Hövelmann, T. M. Stawski, R. Besselink, H. M. Freeman, K. M. Dietmann, S. Mayanna, B. R. Pauw and L. G. Benning, *Nanoscale*, 2019, **11**, 6939–6951.
149 Y. Shi, Y. Wan and D. Zhao, *Chem. Soc. Rev.*, 2011, **40**, 3854–3878.
150 J. Deng, L. Zhang, H. Dai and C.-T. Au, *Appl. Catal., A*, 2009, **352**, 43–49.
151 H. Jiang, T. Zhao, C. Li and J. Ma, *Chem. Commun.*, 2011, **47**, 8590–8592.
152 S. H. Gage, J. Engelhardt, M. J. Menart, C. Ngo, G. J. Leong, Y. Ji, B. G. Trewyn, S. Pylypenko and R. M. Richards, *ACS Omega*, 2018, **3**, 7681–7691.
153 H. Zhu, Y. Chen, Z. Wang, W. Liu and L. Wang, *RSC Adv.*, 2018, **8**, 14888–14897.
154 N. Pal and A. Bhaumik, *RSC Adv.*, 2015, **5**, 24363–24391.
155 X. Wang, Y. Liu, T. Zhang, Y. Luo, Z. Lan, K. Zhang, J. Zuo, L. Jiang and R. Wang, *ACS Catal.*, 2017, **7**, 1626–1636.
156 X. Kang, K. Lyu, L. Li, J. Li, L. Kimberley, B. Wang, L. Liu, Y. Cheng, M. D. Frogley, S. Rudić, A. J. Ramirez-Cuesta, R. A. W. Dryfe, B. Han, S. Yang and M. Schröder, *Nat. Commun.*, 2019, **10**, 4466.